University of Alberta

The Relationship between Ultrasonic Signal and Fatigue Crack Surface Contact in Mild Steel Plate Specimen

by

Che Chien Ng

A thesis submitted to the Faculty of Graduate Studies and Research

in partial fulfillment of the requirements for the degree of

Master of Science

Department of Mechanical Engineering

Edmonton, Alberta

Fall 2008

Library and Archives Canada

Published Heritage Branch

395 Wellington Street
Ottawa ON K1A 0N4
Canada

Bibliothèque et Archives Canada

Direction du Patrimoine de l'édition

395, rue Wellington
Ottawa ON K1A 0N4
Canada

Your file Votre référence
ISBN: 978-0-494-47376-4
Our file Notre référence
ISBN: 978-0-494-47376-4

NOTICE:
The author has granted a non-exclusive license allowing Library and Archives Canada to reproduce, publish, archive, preserve, conserve, communicate to the public by telecommunication or on the Internet, loan, distribute and sell theses worldwide, for commercial or non-commercial purposes, in microform, paper, electronic and/or any other formats.

The author retains copyright ownership and moral rights in this thesis. Neither the thesis nor substantial extracts from it may be printed or otherwise reproduced without the author's permission.

AVIS:
L'auteur a accordé une licence non exclusive permettant à la Bibliothèque et Archives Canada de reproduire, publier, archiver, sauvegarder, conserver, transmettre au public par télécommunication ou par l'Internet, prêter, distribuer et vendre des thèses partout dans le monde, à des fins commerciales ou autres, sur support microforme, papier, électronique et/ou autres formats.

L'auteur conserve la propriété du droit d'auteur et des droits moraux qui protège cette thèse. Ni la thèse ni des extraits substantiels de celle-ci ne doivent être imprimés ou autrement reproduits sans son autorisation.

In compliance with the Canadian Privacy Act some supporting forms may have been removed from this thesis.

While these forms may be included in the document page count, their removal does not represent any loss of content from the thesis.

Conformément à la loi canadienne sur la protection de la vie privée, quelques formulaires secondaires ont été enlevés de cette thèse.

Bien que ces formulaires aient inclus dans la pagination, il n'y aura aucun contenu manquant.

Canada

Abstract

Nondestructive evaluation using ultrasonic waves for crack identification is an important technique in failure prevention of materials and structures. Fatigue cracks usually experience crack surface contact because of the existence of residual stresses near the crack tips. These contacting crack surfaces will reduce the effective length of the crack and, therefore, affect the collected ultrasonic waves.

The current work provides an experimental study of the effect of crack surface contact on the collected ultrasonic signal. Cracked steel specimens were monotonically loaded in compliance testing to estimate their opening load. Ultrasonic shear wave was generated in the specimens and reflection from the crack was measured to estimate the effective crack length under different quasi-static bending moments. By controlling the opening load level, a relationship between the length of crack surface contact and reflected ultrasonic signal was established. Measurement accuracy of these contacting areas is further improved using the proposed graphical solution.

Table of Contents

Chapter 1 Introduction 1

1.1 Background 1

1.2 Scope 2

1.3 Thesis Organization 4

Chapter 2 Literature Review 5

2.1 Crack Closure 6

2.1.1 Introduction to crack closure 6

2.1.2 Measurement of fatigue crack closure 8

2.2 Types of Ultrasonic Waves used in Nondestructive Testing 11

2.3 Application of ultrasonic NDT in fatigue crack closure 14

2.3.1 Ultrasonic longitudinal wave with normal incidence 14

2.3.2 Ultrasonic longitudinal wave with angled incidence 17

2.3.3 Ultrasonic shear wave with normal incidence 21

2.3.4 Ultrasonic shear wave with angled incidence 21

Chapter 3 Compliance Testing for Static Crack Closure 24

3.1 Specimen Preparation 24

3.2 Procedure of Compliance Testing 28

3.3 Analysis of Compliance Test Data 31

Chapter 4 Ultrasonic Testing 44

4.1 Shear Wave Angle Beam with Contact Transducer 44

4.2 Inspection on EDM Specimen 47

4.2.1 Data analysis on crack corner signal 50

4.2.2 Data analysis on crack tip signal 54

4.3 Inspection on Fatigue Crack Specimen 64

4.3.1 Data analysis on crack corner signal at varied load from no load to maximum opening load 65

4.3.2 Data analysis on crack tip signal under various crack opening loads 72

Chapter 5 Conclusion and Future Work 87

References 90

List of Figures

Figure 1: Plastically deformed areas along the crack propagation path [25] 7

Figure 2: Remote and near tip compliance gauges for the measurement of crack closure [22] 9

Figure 3: Typical load – displacement trace [11] 9

Figure 4: Principle of TOFD and generalized geometrical solution [41].....18

Figure 5: Specimen with triangular notch before crack formation.....25

Figure 6: Three point bending of a steel plate specimen on a Vibrophore 25

Figure 7: Schematic of 3-point bending.....27

Figure 8: Specimen setup for compliance test 29

Figure 9: Monotonic loading in compliance testing of specimen CO1 to CO4.....30

Figure 10: Specimen with removed notch. 2-drilled holes were made for loading with screws on the specimen jig 31

Figure 11: Compliance test of specimen CO1 (solid line = recorded data, dash line = fitted line) 32

Figure 12: Compliance test of specimen CO2 (solid line = recorded data, dash line = fitted line) 33

Figure 13: Compliance test of specimen CO3 (solid line = recorded data, dash line = fitted line) 33

Figure 14: Compliance test of specimen CO4 (solid line = recorded data, dash line = fitted line) 34

Figure 15: Variation of compliance with load to determine the crack opening load 35

Figure 16: Compliance offset of specimen CO1 based on ASTM E 647 36
Figure 17: Compliance offset of specimen CO2 based on ASTM E 647 36
Figure 18: Compliance offset of specimen CO3 based on ASTM E 647 37
Figure 19: Compliance offset of specimen CO4 based on ASTM E 647 37
Figure 20: Four-point-bending specimen jig without specimen (a) and with specimen (b).....38
Figure 21: Strain gages on the left and right side of the crack 39
Figure 22 Load vs. strain plots of specimen CO1 under opening load on MTS machine.....40
Figure 23 Load vs. strain plots of specimen CO2 under opening load on MTS machine.....41
Figure 24 Load vs. strain plots of specimen CO3 under opening load on MTS machine.....41
Figure 25 Load vs. strain plots of specimen CO4 under opening load on MTS machine.....42
Figure 26: Feature extraction based on amplitude of an ultrasonic signal.....47
Figure 27: B-scan representation of ultrasonic signal amplitude from a 2.5-mm-deep EDM slot.....50
Figure 28: Echo-dynamics of the fully rectified ultrasonic signal amplitudes from the slot corner of specimen with 1.5-mm-deep EDM slot 51
Figure 29: Echo-dynamics of the fully rectified ultrasonic amplitude of the slot corner of EDM slots with different depths 52

Figure 30: Echo-dynamics of the peak-to-peak ultrasonic signal amplitude of the slot corner of EDM slots with different depths 52
Figure 31: Peak values of ultrasonic signal amplitude from the corner of EDM slots with different depths 53
Figure 32: B-scan result of an EDM specimen with 3.0 mm slot depth at 57.5 dB gain level 55
Figure 33: B-scan result of an EDM specimen with 3.0 mm slot depth at 57.5 dB gain level with grid 56
Figure 34: A-scan display of the ultrasonic signal collected from specimen with 3.0 mm deep EDM slot at the transducer's position of 20 mm. 56
Figure 35: Echo-dynamics of ultrasonic signal diffracted from the crack tip of specimen with 3.0 mm deep EDM slot 57
Figure 36: Echo-dynamics of ultrasonic signal diffracted from the crack tip of specimen with 2.5 mm deep EDM slot 58
Figure 37: Echo-dynamics of ultrasonic signal diffracted from the crack tip of specimen with 2.0 mm deep EDM slot 58
Figure 38: Echo-dynamics of ultrasonic signal diffracted from the crack tip of specimen with 1.5 mm deep EDM slot 59
Figure 39: Graphical representation of the solution for crack depth estimation...61
Figure 40: Extracted amplitude from specimen CO2 at 50% crack opening load65
Figure 41: Extracted peak-to-peak amplitude from specimen CO1 at various crack opening loads.....66

Figure 42: Extracted peak-to-peak amplitude from specimen CO2 at various crack opening loads....67
Figure 43: Extracted peak-to-peak amplitude from specimen CO3 at various crack opening loads....68
Figure 44: Extracted peak-to-peak amplitude from specimen CO4 at various crack opening loads....68
Figure 45: Peak-to-peak amplitude of fatigue cracks at various opening load levels....69
Figure 46: B-scans of specimen CO1 at no load....73
Figure 47: B-scans of specimen CO1 at 25% crack opening load....73
Figure 48: B-scans of specimen CO1 at 50% crack opening load....74
Figure 49: B-scans of specimen CO1 at 75% crack opening load....74
Figure 50: B-scans of specimen CO1 at 100% crack opening load....75
Figure 51: B-scans of specimen CO1 at 105% crack opening load....75
Figure 52: B-scans of specimen CO1 at 110% crack opening load....76
Figure 53: B-scans of specimen CO1 under 110% crack opening load....77
Figure 54: A-Scan of specimen CO1 under 110% crack opening load at probe position 25 mm....77
Figure 55: Extracted tip diffracted signal amplitude of specimen CO1 under 110% opening load....78
Figure 56: Extracted tip diffracted signal amplitude of specimen CO2 under 110% opening load....79

Figure 57: Extracted tip diffracted signal amplitude of specimen CO3 under 110% opening load 79

Figure 58: Echo-dynamics of ultrasonic signal diffracted by the crack tip of specimen CO1 under 0% crack opening load 83

Figure 59: Echo-dynamics of ultrasonic signal diffracted by the crack tip of specimen CO2 under 50% crack opening load 84

Figure 60: Echo-dynamics of ultrasonic signal diffracted by the crack tip of specimen CO3 under 50% crack opening load 84

List of Tables

Table 1: Loading sequence for a crack propagation up to 4 mm with initial notch depth of 5 mm....28

Table 2: Specimens' loading condition for compliance testing....29

Table 3 Estimated opening load based on least-square method....34

Table 4: Estimated EDM depth using the calibrated axis of Omniscan UT....60

Table 5: Estimated EDM depths based on graphical solution....63

Table 6: Fatigue crack depth estimation based on linear fitting of EDM specimens peak-to-peak amplitude of the ultrasonic signal reflected by the EDM slot corner....71

Table 7: Estimated fatigue crack depths under 100% crack opening load based on the calibrated axis of the Omniscan UT....81

Table 8: Estimated fatigue crack depths under 100% crack opening load using graphical solution....82

Table 9: Estimated crack depths under loading condition lower than 50% using graphical solution....85

Chapter 1 Introduction

1.1 Background

Nondestructive evaluation or NDE refers to the evaluation of the integrity and reliability of a structure without doing any harm or destroying the object under scrutiny. Up to this point, there have been several different techniques of NDE based on the medium used for evaluation. One of the widely utilized NDE methods is the use of ultrasonic elastic waves to identify, locate and measure defects that exist on the surface or within a structure. Such an application is made possible by the use of piezoelectric material that acts as the source of ultrasonic vibration when it is excited by an electric field. This piezoelectric material is typically encased within a package and is commonly know as ultrasonic transducer.

The applications of ultrasonic NDE range across different types of inspected materials from metallic objects including railroads and pipelines to nonmetals such as woods and human tissues. The importance of NDE can be easily seen from these examples. With fossil fuels still remain as the crucial driving force in industries around the world, the integrity of pipeline structures as the main oil and gas transporting instrument plays a key role in ensuring its uninterrupted delivery. On the other hand, a well-conditioned railroad is one important aspect that allows the train to reliably transport human being and commodities from one location to another. Two of the commonly found defects in pipeline structure and railroads are corrosion and cracks.

Corrosion affects pipeline by reducing the available wall thickness to contain the pressure from within the pipe. In the case of railroads, corrosion reduces the cross section of the rail and thus, reduces the strength of the rail. Moreover, corrosion can lead to the formation of pitting which acts as the stress concentration. Corrosion inspection usually involves the application of ultrasonic thickness gauges.

On the other hand, the effect of cracks on a structure depends on the loading history experienced by that particular structure. Its detection and sizing are more complicated than inspecting corrosion because it involves the location, condition and geometry of the crack. One obvious aspect involving the state of a crack is its depth because it may be a deciding factor on whether or not a structure is deemed as sufficiently safe to remain in-service. At this point, ultrasonic NDE will include not only crack detection but also crack sizing. The main problem with crack sizing either on the basis of fracture mechanics or ultrasonic NDE is the phenomenon of crack closure or crack surface contact. In its effect on ultrasonic, the existence of crack surface contact will cause the ultrasonic wave to pass through those contact points or areas rather than be reflected to the transducers as defect indications. As a result, those areas where crack surfaces contact each other will appear to be defect-free and the measurement result will be inaccurate.

1.2 Scope

The objective of this thesis is to evaluate the behavior of ultrasonic signal upon the existence of crack surface contact. Primary focus is given to the earlier stage

of mechanically developed crack contact in plate specimen. The investigated fatigue cracks depths range from 6% to 25 % of the wall thickness. The crack surface contact will be assessed from the point of view of fracture mechanics and the principle of ultrasonic NDE and evaluation of the crack conditions is conducted on the basis of experimental data collected using both fatigue testing machine and ultrasonic flaw detectors.

The phenomenon of crack surface contact was first studied in the field of fracture mechanics by Elber in 1968 and the study on fatigue crack has drastically changed since then. It seems that crack surface contact is an inseparable component needed to analyze fatigue crack sufficiently [36]. In this study, the ultrasonic NDE is conducted using a single transducer and two key parameters of the collected signal, e.g., amplitude and time-of-flight, are analyzed. In order to study the effect of crack surface contact, various level of static load is applied to the test specimen to simulate different levels of crack surface contact until the crack is fully opened. At each level, ultrasonic data is collected and the effect of different values of externally applied closure stress on the amplitude of the first ultrasonic signal reflected from the corner of the crack and diffracted from the tip of the crack will be evaluated.

Another method for crack measurement is based on the diffraction phenomenon that takes place at the extremities of a crack. It does not rely on the amplitude of the ultrasonic to assess a discontinuity, instead it uses only the time-of-flight or traveling time of the collected ultrasonic signal. In this thesis, the resulting assessment from both amplitude and time-of-flight based method will be

compared to investigate the effect of crack surface contact on the recorded ultrasonic signal.

1.3 Thesis Organization

This thesis is organized as follows. In Chapter 2, existing literature surrounding the investigation of crack surface contact from the field of fracture mechanics and ultrasonic nondestructive evaluation is reviewed. Different principles and general setups of ultrasonic methods will be explained in this section, as well. Chapter 3 describes the specimen preparation process including the steps taken to introduce fatigue crack onto the steel specimens and crack assessment based on fracture mechanics. All aspects regarding the ultrasonic nondestructive testing conducted for this study; analysis and discussion of the collected data are presented in Chapter 4. Finally, Chapter 5 provides the conclusion of this thesis and future recommendations.

Chapter 2 Literature Review

One way to ensure the longevity of the service life of engineering structures and to prevent their breakdown is scheduled inspection. Ultrasonics is one example of nondestructive inspection methods. It has been widely and successfully applied to investigate the condition of different components such as integrity of pipeline structure and connections, railroad, building structures and airplane wings [43].

With the unknown internal conditions of the inspected structure, detection and sizing of flaw from the collected signal are usually conducted by comparing it with the ultrasonic signal obtained from a test specimen with similar materials having artificial defects of known location and geometry. However, in the case of fatigue cracks appearing in these structures, there exists certain amount of crack closure or contacting area between crack surfaces near the crack tip [36]. This phenomenon makes the crack partially invisible to ultrasonic signal because the contacting surfaces will allow the ultrasonic signal to pass through and as a result, such a crack will be erroneously measured.

In this chapter, literatures related to crack surface contact, basics of ultrasonic and applications of ultrasonic NDE of crack closure will be reviewed separately. The first section, which focuses on crack closure, provides the background of crack closure including its discovery and how it occurs. It is followed by the review of compliance method that is used to estimate the extent of fatigue crack closure and types of gauges used for this method. The second section reviews

the types of ultrasonic waves that are typically used in ultrasonic NDE and the characteristics of each wave. Finally, the last section of chapter 2 provides the review of different techniques of ultrasonic NDE, mainly the use of longitudinal and shear waves to investigate fatigue crack surface contact.

2.1 Crack Closure

2.1.1 Introduction to crack closure

The concept of fatigue crack closure was first studied by Elber in 1968 [21] [36]. It was discovered that opposing surfaces of fatigue crack come into contact with each other during cyclic loading. This phenomenon was observed not only in the tension-compression loading, but also in the tension-tension cyclic loading. Elber established the existence of plastic deformation near the tip of a fatigue crack that leads to crack closure by studying the nonlinearity of crack opening behavior. This is the first mechanism of crack closure and is referred to as plasticity induced closure. Since then, different closure mechanisms have been identified, such as: crack-filling closure and roughness-induced closure. The first one occurs due to corrosion agents and oxides while the latter is due to the mismatch of opposing crack surface features [27].

One of the most important factors contributing to crack surface contact is the formation of plastic region at the area near the crack tip caused by fatigue loading [13] [24] [25]. There are two different plastic zones formed during different phases of fatigue loading. As the load increases at each loading cycle, a monotonic plastic zone is formed at the tip of propagating fatigue crack, as

shown in Figure 1(a). It is subsequently followed by the formation of a smaller cyclic plastic zone during the unloading phase of every cycle. The size of the cyclic plastic zone is approximately a quarter of the monotonic plastic zone, as seen in Figure 1(b). As the crack propagates, it will leave behind a region of monotonically stretched area along and perpendicular to the crack flank as shown in Figure 1(c) and Figure 1(d). Since the area around this region remains elastic, it will generate residual stresses on this plastic region as the fatigue load decreases. Hence, the crack will tend to close.

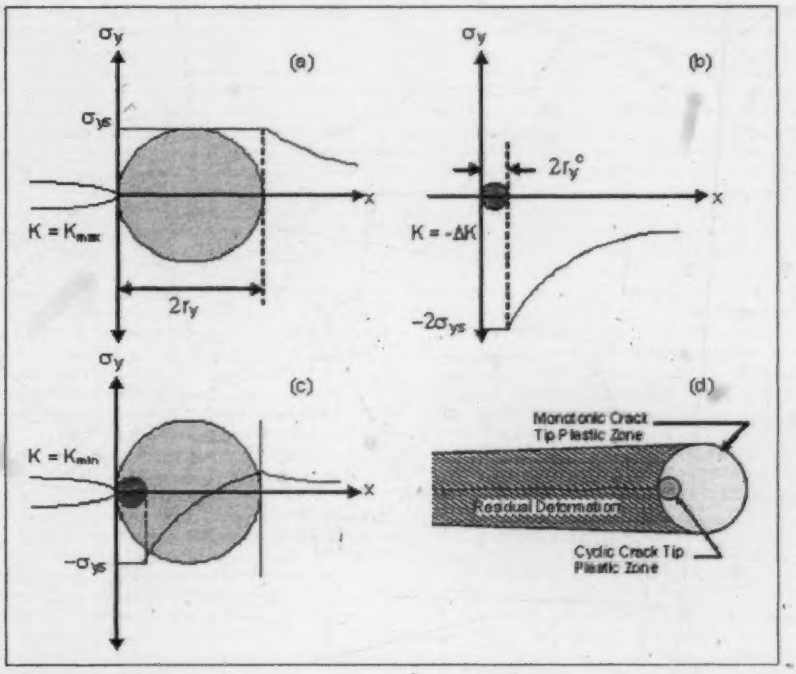

Figure 1: Plastically deformed areas along the crack propagation path [25]

2.1.2 Measurement of fatigue crack closure

One of the standard techniques to measure the crack closure is compliance method [22]. This method evaluates the extent of crack closure by detecting the decrease in compliance value of a cracked structure. Compliance of a structure, C, is the inverse of its stiffness, k, and thus, is formulated as [25]:

$$C = \frac{1}{k} = \frac{\delta}{P} \qquad (1)$$

in which P is the applied load at the loading point and δ is the displacement.

The change of compliance can be generally expressed as the inverse gradient of the line connecting 2 data points in the load-strain data:

$$Change\ of\ compliance = \frac{\Delta\delta}{\Delta P} \qquad (2)$$

Two different types of gauges can be used to obtain the load vs. displacement data for crack closure response measurement. The first category of gauges is placed remotely from the crack tip and hence, is more often used to measure crack length and monitor only the bulk response of crack closure. Crack mouth gauge and back face strain gauge are the most commonly used remote gauges. The second type of compliance gauges is installed at a location near the tip of the crack and therefore, is more sensitive to crack closure. These gauges include the near tip displacement gauge and near tip strain gauge. The applications of both types of gauges can be seen in Figure 2. There are different ways to determine the crack opening load from the load vs. displacement data collected with the gauges. The opening load is defined as the minimum load during the

fatigue cycle at which there is no crack surface contact [14]. A typical load – displacement trace, as shown in Figure 3, can be dissected into different sections.

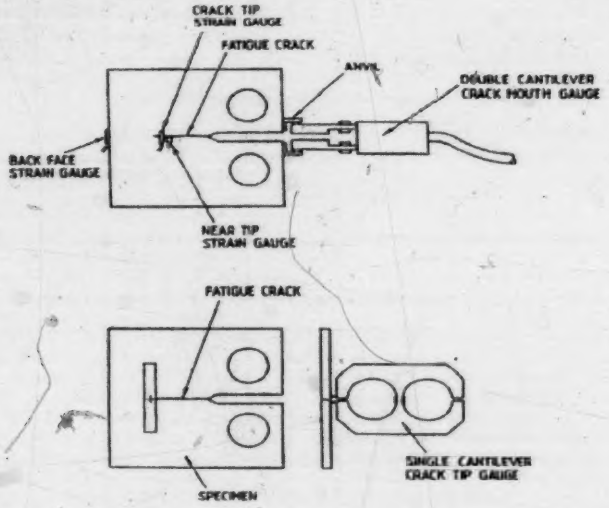

Figure 2: Remote and near tip compliance gauges for the measurement of crack closure [22]

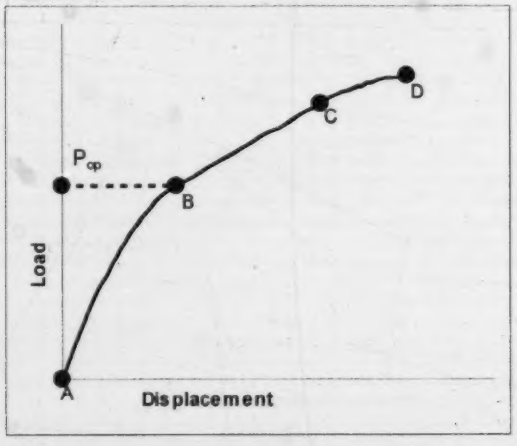

Figure 3: Typical load – displacement trace [11]

Region AB shows the displacement change to the applied load when the crack is in the process of opening. In this stage, compliance of the specimen will continually increase up to point B. This point marks the change in the load-displacement trace where the curve becomes linear and becomes the accepted notion of determining crack opening load, P_{op}. At this time, the crack has been fully opened, the measured displacement will conform to the linear elastic behavior of the material and there will not be any crack growth until it reaches point C. Beyond point C, higher loads will introduce significant plastic deformation onto the material and promote further crack growth.

There have been different methods proposed to determine the crack opening load from the load-displacement data. Carman, Turner and Hillberry [14] used the load – reduced displacement curve obtained with a crack tip opening displacement gauge to estimate the opening load. This curve is obtained by extrapolating the linear part of the original load-displacement data and subtracting it from the displacement data in a regressing manner. They found that the non-linear portion of the load-displacement data, i.e., crack opening phase is of second order. Donald [18] suggested the use of 2% slope offset of the load – displacement data to determine the crack opening load. This technique is then added to the standardized testing method, ASTM E 647 "Recommended Practice for Determination of Fatigue Crack Opening Load from Compliance" in which 2% is set as the minimum offset value to estimate the crack opening load [19]. More details on this method will be provided in Chapter 3.

2.2 Types of Ultrasonic Waves used in Nondestructive Testing

The ultrasonic nondestructive testing is developed on the basis that solid material is an excellent medium for wave propagation. Upon exiting the transducer, the ultrasonic waves will be reflected either by material interfaces or internal flaws. These waves carry the information regarding the conditions of the reflection source to the receiving transducer. If the reflection source is the material interface, one will be able to estimate the geometry of the interface and measure the distance of that interface relative to the transmitter and/or receiver. On the other hand, if ultrasonic waves are reflected by internal flaws such as inclusions and cracks, the reflected ultrasonic waves will contain information regarding the flaws dimensions. Therefore, applications of ultrasonic nondestructive testing (NDT) can be found in thickness measurement, defect detection and sizing.

Generally, there are two different types of waves utilized in ultrasonic NDT. The first one is longitudinal wave and the second one is transverse/shear wave. Longitudinal wave is defined as a wave whose displacement is parallel to its propagating direction. The displacement of shear wave is perpendicular to the direction of propagation. In their relation to ultrasonic NDT, the characteristics of these waves are also different. With its higher wave speed (and thus, shorter wave length), longitudinal wave is less prone to attenuation than shear wave. This makes longitudinal wave transducer more suitable to inspect highly attenuative material. However, for the same reason, shear wave transducer is properly suited to the inspection whose main factor is resolution. Due to its slower wave speed (approximately half of longitudinal wave), the peaks of shear

wave reflections from the extremities of a small defect, e.g., tips of a short crack, are located further from each other so that the crack will not be misidentified for an inclusion.

Based on the direction the ultrasonic waves entering the material, ultrasonic NDT can also be divided into two different categories: normal beam and angle beam inspections. In normal beam, the ultrasonic waves are introduced to and travel inside the specimen perpendicular to the material surface or 0^0 to the normal of the inspected surface. This technique is commonly used for thickness measurement, corrosion measurement/mapping and inspection of internal defects especially planar cracks. On the other hand, angle beam inspection introduces the ultrasonic wave at angles other than the normal orientation of the inspected surface. A wedge is usually attached to the transducer to allow the ultrasonic wave to enter the material at certain angle. This method is usually used for defect detection and measurement. Note that, orientation of the defect, especially cracks, plays a role in determining the most suitable method. Crack inspection with normal beam is best suited when the crack is oriented parallel to the inspection surface. However, when the crack is vertical to the inspection surface, angle beam will produce better accuracy.

Depending on the incident angle, the angle beam configuration will produce different propagating waves inside the inspected material. Upon further development of the ultrasonic NDT, another type of propagating wave generated using the angle beam setup, called guided wave, was discovered. Guided wave is an ultrasonic wave whose propagation is directed by the boundary of the

inspected specimen. When a guided wave is generated on a single boundary, its propagation is bounded to a surface and is usually known as surface acoustic wave (SAW). In order to generate surface wave, certain wedge angle is selected to produce an ultrasonic wave that is incident to the inspected material at 90^0. On the boundary between solid-air, solid-liquid and solid-solid, surface acoustic waves generated are Rayleigh, Scholte and Stoneley waves, respectively. As its name suggests, the surface acoustic waves travel only on the surface of the inspected material. They can only detect defects that are located on or close to the scanning surface of the specimen because its amplitude will reduce to one twenty fifth of the initial value at a depth of one wavelength [29]. On the other hand, when an ultrasonic wave is guided by two parallel boundaries that reflect the angled incident waves multiple times, it leads to the interference among the reflected waves and resonant waves and is called Lamb waves [37]. Due to this resonance, Lamb waves are typically used for long range inspection where an ultrasonic transducer can not be positioned in the vicinity of the defect. Other application of Lamb waves is to evaluate the quality of lamination of thin materials [29]. In this thesis, focus will be given primarily on the use of bulk ultrasonic waves, that are longitudinal and shear waves, and the reported investigations on crack closure using these two ultrasonic waves will be presented in the next section.

2.3 Application of ultrasonic NDT in fatigue crack closure

2.3.1 Ultrasonic longitudinal wave with normal incidence

Longitudinal normal beam transducers can be used in either pulse-echo or through-transmission configurations. In pulse-echo, a single transducer will emit ultrasonic pulses and collect the reflected echoes. On the other hand, through-transmission method requires at least one pair of transducers in which one will be the transmitting transducer and another functions as the receiving transducer that is placed at the opposite face of the transmitter to collect the incoming ultrasonic wave. Additional transmitters or receivers can be added to increase coverage area. As previously mentioned, normal beam inspection is used mainly for horizontal crack detection, thickness and corrosion measurement. All these applications rely on the reflected signal from either crack surface or material interface. When ultrasonic wave is reflected, the direction of the reflected wave depends on the incident angle. According to the law of reflection, ultrasonic wave will be reflected by a boundary at an identical angle to its angle of incidence measured from the normal of that boundary. Thus, In the case of transducer with normal orientation, the reflected waves return in the same propagation path as the incident wave.

Using the through-transmission method to investigate crack closure, Buck et al. [12] discovered the effect of a crack's loading history on the transmission coefficient of the ultrasonic signal. Other than the observed contacting crack surface area near the crack tip of aluminum 7075-T651 specimens, the transmission coefficient shows another contacting area away from the crack tip.

The second contact area between the crack surfaces was suspected to occur due to the additional fatigue loading applied to the specimen resulting in the original crack to propagate another 10 mm. Hence, the first peak of the transmission coefficient represents the current crack depth and the second peak indicated that crack surface contact may remain even though the crack has propagated further.

Rehbein et al. [12] [31] utilized the longitudinal through-transmission method to study the effect of contacts between the opposing surfaces of fatigue crack on ultrasonic wave transmission. One transmitting and two receiving transducers are used in their experiments. The first receiver is located in alignment with the transmitter as in normal through transmission. On the other hand, the second receiver is placed on the same side as the first receiver to obtain the signal diffracted from the crack tip with a 45-degree angle of reception. Diffraction is different from reflection in a way it responds to an incoming ultrasonic wave. While the direction of reflected wave is dependent on the relative orientation between the incident wave and the crack, diffracted wave propagates in all directions upon contact between the incident wave and extremities of a defect and is independent of crack orientation [38].

Three aluminum 2024-T351 specimens whose fatigue cracks developed under different conditions were investigated. The first crack propagated under loading with constant stress intensity factor and was overloaded for 21 cycles. The second one propagated under constant stress intensity factor and was overloaded for a single cycle. The last crack grew under the condition of

continually decreasing stress intensity factor that leads to continual decrease of crack growth rate [12] [31]. The through-transmission signal shows that the occurrence of crack surface contact can be observed from all specimens using the transmission coefficient. A transmission coefficient of 1 refers to a full ultrasonic transmission [20], while anything between 0 and 1 represent certain amount of contact between the crack surfaces. When the crack is fully opened, the ultrasonic signal will not be able to reach the transmitter because it is completely reflected by the crack surface and thus, the transmission coefficient will be zero.

The overloaded specimens produce very low transmission coefficient along the crack surface and one peak corresponding to the crack tip is observed. The peak's transmission reflection value is higher in the specimen overloaded for 21 cycles than that for single cycle. This leads to the conclusion that overloading the specimen leads to the formation of additional plastic deformation zone that increases the contacting crack surface allowing the ultrasonic wave to be transmitted to the receiver. The specimen loaded with decreasing stress intensity factor shows a partial crack surface contact along the crack length and it is depicted by a transmission coefficient value that is higher than the fatigue crack developed under constant stress intensity factor. From the comparison between these two specimens, loading history, i.e., the difference in stress intensity factor values used during crack growth, has shown to play an important role in the generation of plastic zone at the crack wake area which directly affects the extent of crack surface contact. The result is further confirmed by appearance of several

diffracted signals obtained from the overloaded specimen other than the crack tip signals. These multiple diffracted signals originate from the ultrasonic waves that pass through the area where crack surfaces come into contact with each other and signify the occurrence of crack surface contact behind the crack tip [12] [31]. Saka with Abe [32] and Uchikawa [35] used the normal beam longitudinal wave transducer in a pulse-echo configuration to investigate the effect of crack closure in stainless steel AISI304 specimens on ultrasonic signals. Fatigue cracks were generated vertically at the opposite side of the scanning surface and the stress intensity factor and stress ratio were maintained constant during crack propagation. By comparing the normalized amplitudes of two specimens with almost similar fatigue crack depth developed under identical stress intensity factor and different stress ratio, the shape of the plotted amplitudes along the scanning line are completely different. Therefore, it can be concluded that loading history, including stress intensity factor and stress ratio, plays an important role in the degree of crack surface contact in fatigue cracks and inclusion of crack closure in the analysis of fatigue crack is a necessity in order to achieve more accurate defect sizing.

2.3.2 Ultrasonic longitudinal wave with angled incidence

The use of angle beam longitudinal wave transducers for ultrasonic NDT is commonly found in the Time-of-Flight-Diffraction (TOFD) method. In this method, two transducers are placed on the same inspection surface and facing one another. This kind of transducer setup, also known as pitch-catch configuration,

requires one probe to be the transmitter and another as the receiver. This technique was founded by Silk [38]-[42] in the early 1970s. As the name suggests, TOFD utilizes only time-of-flight of the tip-diffracted ultrasonic signals to detect the existence of flaws and measure their dimensions [10]. The difference in the defect location or sizing estimation between angle beam and normal beam is the non-linearity of the relationship between time-of-flight and defect position and this is due to the way ultrasonic wave propagates within the material. The basic concept of TOFD and the general solution for crack tip location are depicted in the Figure 4.

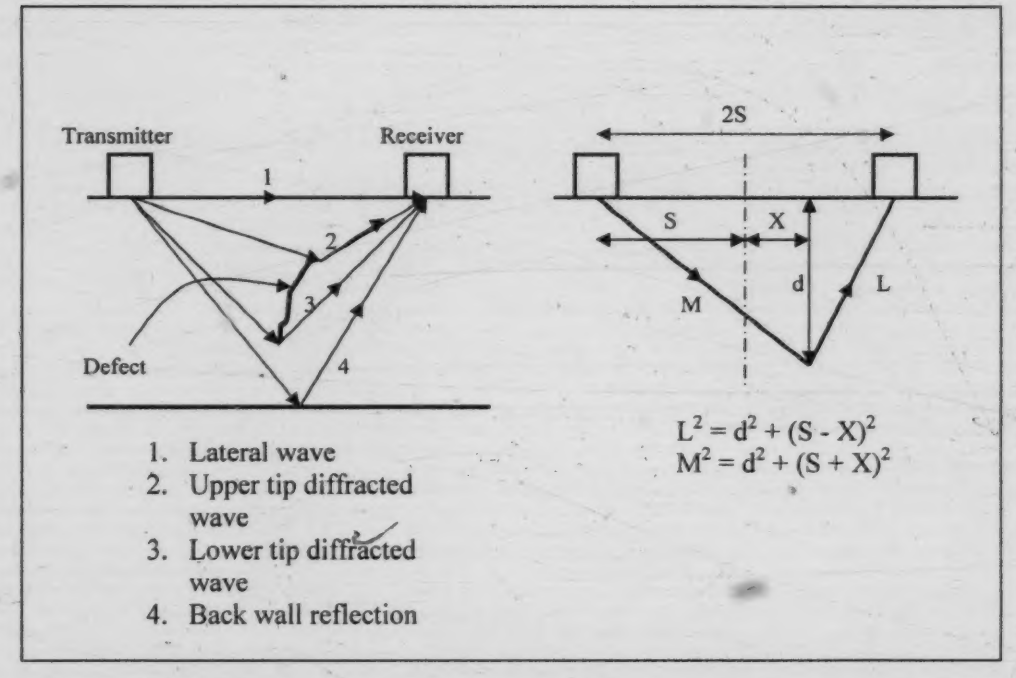

Figure 4: Principle of TOFD and generalized geometrical solution [41]

It can be seen from Figure 4 that moving the transducer over the crack will lead to different path of ultrasonic wave propagation. However, the general solution

remains the same due to the omni-directional characteristics of tip-diffracted wave. Hence, the length of wave propagation path within the specimen can be formulated as:

$$M + L = [d^2 + (S + X)^2]^{1/2} + [d^2 + (S - X)^2]^{1/2} \quad (3)$$

Differentiating this formula shows that the shortest wave propagation path is obtained when the crack tip is located exactly in the middle between the transducers or X = 0. Under this condition, the formula for the length of wave propagation path within the specimen becomes:

$$M + L = 2 \times [d^2 + S^2]^{1/2} \quad (4)$$

Thus, the crack tip location, d, can be calculated when the length of wave propagation path of the ultrasonic signal within the specimen and the probe separation distance are known. The length of ultrasonic wave propagation path is calculated by multiplying the recorded time of flight to the material sound velocity. The probe separation distance is measured from the beam index points of the transmitter to the receiver. Beam index point is the position at which the ultrasonic wave exits the probe. The experimental investigation on fatigue cracks conducted by Lidington et al. [26] found that TOFD is capable of sizing these cracks with a mean accuracy better than 0.5 mm. Chen et al. [15] used the same TOFD technique on 12-mm-thick steel plates of different depths of EDM slots. The error in measurement ranges from 0.06 mm to a maximum of 0.28 mm. Furthermore, they improved the TOFD based measurement by utilizing empirical mode decomposition and as a result, the measurement error decreases by at

least 50%. Using this configuration, Mihara et al. concluded that the ultrasonic signal diffracted by the crack tip gradually intensifies as the crack tip opening displacement increases and the fully opened crack tip amplitude values approach to those of EDM slots [28].

Ahmed and Saka [1] - [6] took a different approach in the angle beam longitudinal wave inspection. Instead of relying on the tip diffracted signal, they utilize the first signal due to the back wall reflection of a stainless steel AISI304 specimen with closed fatigue crack. The angle at which the ultrasonic wave propagates inside the material is varied from $0 - 15^0$ (small angle) and $30 - 60^0$ (large angle). From the small angle investigations, it was found that by changing the incident angle, the behavior of normalized amplitudes also changes. As the incident angle inside the steel plate is increased from 0 to 15^0, the plotted signal displays increasing amplitude of the ultrasonic wave reflected by the crack corner and adversely, the ultrasonic signal originating from the crack tip experienced declining amplitude. The optimum incident angle of this configuration is about 8^0 for the reason that both the effect from the crack corner and crack tip can be observed clearly and their amplitudes change accordingly with crack depth. At incident angle greater than 8^0, the normalized amplitude of the crack tip signal decreases and only the corner reflection was found on the plot. This optimum angle is selected on the basis that it produces the maximum changes when analyzed signals from different crack depths are compared.

2.3.3 Ultrasonic shear wave with normal incidence

Although the typical uses of ultrasonic shear normal beam are to estimate the shear wave material sound velocity and grain structure characterization, Saka, Schneider and Holler [34] use this method to detect and determine the size of vertically oriented fatigue cracks with time of flight being the parameter of interest. In their investigation, they find that the back wall signal's time of flight of a fatigue crack is longer than EDM slot. By removing the fatigue crack with EDM while keeping the surrounding plastic zone, they find that the time of flight is between those of EDM and the fatigue crack and thus, conclude that the existence of plastic zone surrounding the crack surface affects the time of flight of normal beam shear wave inspection.

2.3.4 Ultrasonic shear wave with angled incidence

Ciorau et al. [16] used TOFD in two different configurations to inspect fatigue cracks in pipe welds. The first configuration is the basic TOFD depicted in Figure 4 and the second one is the pulse-echo based TOFD using one transducer as transmitter and receiver. Using 2.25 MHz, 12.7 mm probe at 45^0, they found that amplitude-based sizing of flaws greater than 4mm is not reliable and higher gain level is necessary to detect the tip of a defect. This limit in measurement accuracy can be attributed to the size difference between the transducer and the inspected defect. When defect is measured on the basis of amplitude, it relies on the principle of wave reflection. Therefore, when the size of a defect approaches or is larger than one half the width of the incident ultrasonic beam, the amount of

ultrasonic signal reflected back to the transducer remains the same and the collected signal will shows identical maximum amplitude.

Different techniques were used to estimate the tip position. The first one is Relative Arrival Time Technique (RATT). It measured the TOF difference between the crack corner and the crack tip. The minimum reported error of this technique is 1 mm [16]. The second method measures the absolute TOF of the tip signal, after the gain level is increased to maximize the tip-diffracted wave amplitude. The tip location estimated results for vertical crack is more accurate when RATT is used. A comparison between 45^0 and 60^0 incident angle shows that 45^0 displays stronger amplitude but the tip-diffracted TOF is more accurate with 60^0.

Akanda and Saka [7] also utilized pulse-echo based shear wave angle beam to investigate crack surface contact in stainless steel AISI304 plates. The difference compared to Ciorau et al. [16] is in the analyzed signal. Akanda and Saka measured only the amplitude of first back wall reflection. Three different incident angles tested include 40^0, 50^0 and 65^0. Normalized amplitudes of 40^0 and 50^0 incident angle produce good correlations between signal amplitudes and EDM slot depths. The use of 50^0 incident angle is found to be the optimum angle for shear wave because it shows a larger change in amplitude between smallest (0.25 mm) and largest (3 mm) slot depths. Also, it is observed that the maximum slot depth that can be inspected with 40^0 incident angle is 2 mm because the normalized amplitude obtained from the 2-mm slot is equal to that from the 3-mm slot. Finally, the 65^0 incident angle shows poor correlation between slot depth

and signal amplitude. The peak of the normalized amplitude can not be identified reliably as it spans over a longer distance of probe position with almost equal amplitude. Thus, using the 50^0 incident angle, the ultrasonic inspection is conducted under different levels of crack closing load and the reflection coefficient of the ultrasonic signal reflected from the corner of the crack is found to decrease in a non-linear manner as crack closure stress increases.

As described above, there are different ultrasonic NDE methods can be used for crack detection and sizing. However, the detectability of the defect greatly depends on the configuration of the ultrasonic inspection being used. In the next chapter, the specimen preparation and experiment conducted prior to the ultrasonic inspection will be presented in details.

Chapter 3 Compliance Testing for Static Crack Closure

This chapter is devoted to presenting the preparation procedure of the specimen for the ultrasonic inspection. The initial step is generating a fatigue crack on a mild steel specimen under controlled parameters including stress intensity factor and stress ratio. Following the crack generation, the compliance value of each specimen is evaluated in order to estimate the amount of crack opening load. Two different methods are presented in the second section. At the end of this chapter, the data analysis conducted to estimate the crack opening load values is presented.

3.1 Specimen Preparation

Material selected is 4140 steel as this type is the most common steel used in various applications such as: axle and crankshaft of automobiles and fittings for pipeline. The raw material arrived in annealed condition and it was learned that annealed steel will generally have large grain size. In relation with ultrasonic NDT, specimen with larger grain size will theoretically lead to more distortion in its signal. Hence, after the raw material was cut to specified dimensions (180 mm x 40 mm x 20 mm), the steel blocks were sent to Thermex Metal Treating Ltd. for heat treatment in order to reduce the grain size. There are three options of heat treatment available: annealing, HRC 18-22 (Rockwell hardness within the range

of 18 to 22) and HRC 28-32. The steel blocks were heat treated to reach a hardness level around HRC 18-22 rather than HRC 28-32 so that they are easier to be machined and for the crack to propagate.

Next, on each specimen, a 4-mm-deep and 2-mm-wide triangular notch was introduced along the specimen width to initiate the crack propagation. The notch was manufactured with a cutter and its tip was further sharpened by EDM (Electrode Discharge Machining). The specimen is shown in Figure 5.

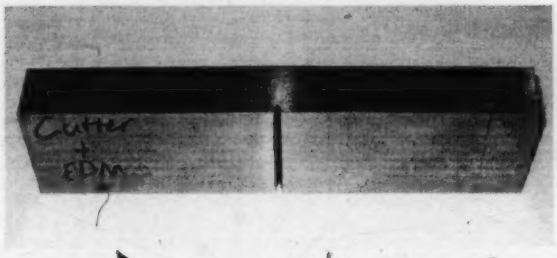

Figure 5: Specimen with triangular notch before crack formation

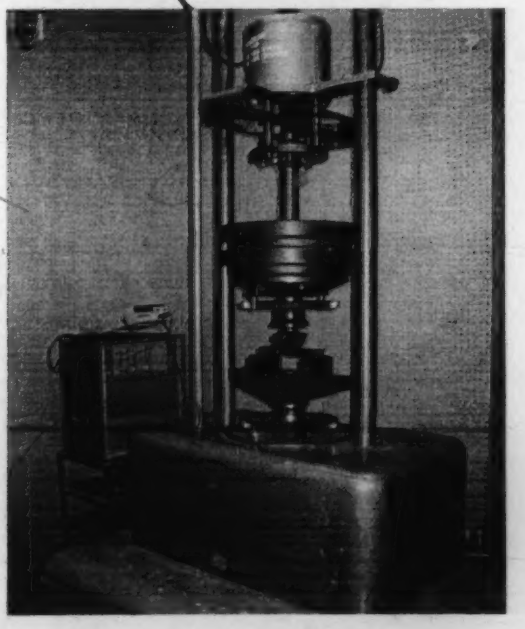

Figure 6: Three point bending of a steel plate specimen on a Vibrophore

Each specimen was subjected to 3-point-bending on an Amsler 10 HFP 422 Vibrophore as shown in Figure 6. It is a resonance-based fatigue testing machine that is capable of high frequency (>100 MHz) loading. This machine was preferred to a regular fatigue testing machine because high frequency fatigue will lead to a more uniform crack depth along the specimen width and faster crack propagation. All specimens were loaded at a frequency of 120 MHz. All four specimens' loading conditions, i.e., mean and amplitude of the load, were estimated based on a stress intensity factor (SIF) of 25 and a load ratio (between minimum and maximum loads) of 0.5. The 3-point-bending maximum load level was estimated using the stress intensity factor formula shown in equation (5) and the schematic of the setup is depicted in Figure 7 [11].

$$K_I = \frac{P}{B\sqrt{w}}\left[\frac{3\frac{s}{w}\sqrt{\frac{a}{w}}}{2\left(1+2\frac{a}{w}\right)\left(1-\frac{a}{w}\right)^{\frac{3}{2}}}\left\{1.99-\frac{a}{w}\left(1-\frac{a}{w}\right)\left[2.15-3.93\frac{a}{w}+2.7\left(\frac{a}{w}\right)^2\right]\right\}\right] \qquad (5)$$

where:

K_I = Stress intensity factor

P = Load

B = Specimen's width

w = Specimen's thickness

a = Crack's depth

s = Distance between supports

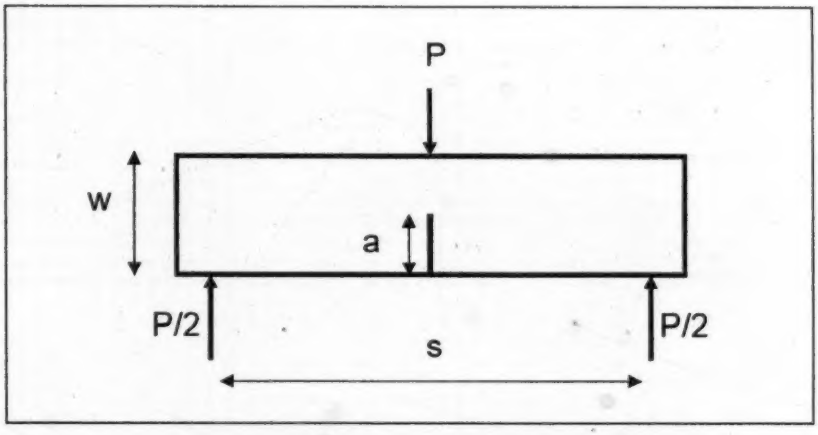

Figure 7: Schematic of 3-point bending

Prior to the actual crack formation on the specimens, two identical test pieces were loaded on the machine to estimate the crack propagation rate, i.e., the number of cycles required by the crack to propagate to a certain depth. Crack depths were inspected using an optical comparator for every 0.25-mm of propagation on both sides of the specimen. The average value of crack depths from both sides was used to adjust the load level according to equation (5) to keep a constant maximum stress intensity factor of 25 and load ratio of 0.5. The sample of load adjustments during crack propagation can be observed in the Table 1.

a [mm] (Fatigue Crack Depth)	P_{max} [kN]	P_{mean} [kN]	Loading Amplitude (+/-) [kN]
5	18.97051204	14.22788403	4.742628011
5.25	18.63894405	13.97920804	4.659736013
5.5	18.31544937	13.73658703	4.578862343

5.75	17.9984819	13.49886143	4.499620476
6	17.68679009	13.26509257	4.421697522
6.25	17.37935792	13.03451844	4.34483948
6.5	17.0753585	12.80651888	4.268839626
6.75	16.77411715	12.58058786	4.193529287
7	16.47508186	12.3563114	4.118770465
7.25	16.17779954	12.13334965	4.044449884
7.5	15.88189669	11.91142252	3.970474174
7.75	15.58706378	11.69029783	3.896765945
8	15.29304237	11.46978178	3.823260592
8.25	14.99961469	11.24971102	3.749903673
8.5	14.70659507	11.0299463	3.676648766
8.75	14.41382286	10.81036715	3.603455716
9	14.12115678	10.59086758	3.530289194

Table 1: Loading sequence for a crack propagation up to 4 mm with initial notch depth of 5 mm

3.2 Procedure of Compliance Testing

Crack developed through fatigue process often has certain amount of closure between its surfaces. The crack opening load can be determined by means of compliance testing. For each specimen, a strain gage is attached straddling the notch (see Figure 8). Next, a monotonically increasing load is applied to the specimen using the 3-point bending fixture as when the fatigue crack is

introduced to the specimen. The stress vs. strain curve is plotted and the load is increased to just under the lower level of last load value applied during the crack propagation process, i.e., P_{mean} – Loading Amplitude. In total, there are 4 specimens made and they are labeled as CO1 to CO4 to indicate the fatigue crack depth from the deepest to the shallowest, respectively. The loading condition for each specimen is shown in Table 2. This was done so that there would not be any alteration to the crack conditions, i.e., no further crack propagations. The use of silicon gel under the strain gage is to provide a foundation for the strain gage and prevent it from buckling.

Specimen	Measured Fatigue crack Depth [mm]	Mean Load of Last Step [kN]	Load Amplitude of Last Step [+/- kN]	Maximum Load in Compliance Testing [kN]
CO1	3.8735	10.96	3.6	7
CO2	3.048	11.47	3.81	7
CO3	2.0955	12.56	4.19	8
CO4	1.016	13.5	4.5	8

Table 2: Specimens' loading condition for compliance testing

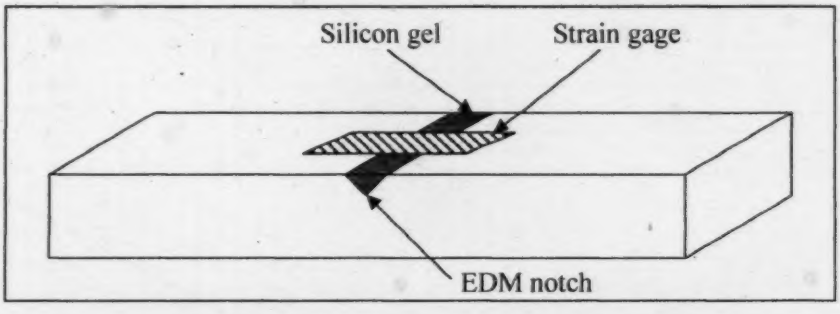

Figure 8: Specimen setup for compliance test

Note that, since every specimen has different crack depth, the final load recorded during fatigue test is different for each specimen. The recorded data of the compliance testing are plotted in Figure 9. After completing the compliance test on all 4 specimens, the notches are completely removed by milling and the surfaces were ground. Thus, every specimen has only a true fatigue surface crack left. Additionally, two through holes were made for mounting the specimen to the specimen jig for ultrasonic inspection. The finished specimen is shown in Figure 10.

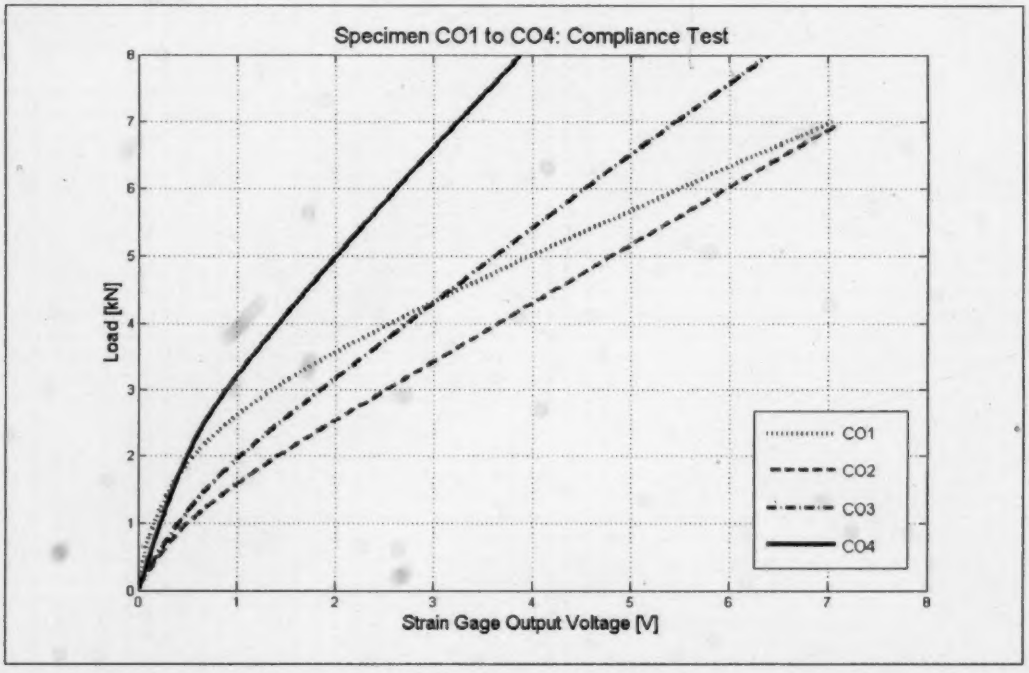

Figure 9: Monotonic loading in compliance testing of specimen CO1 to CO4

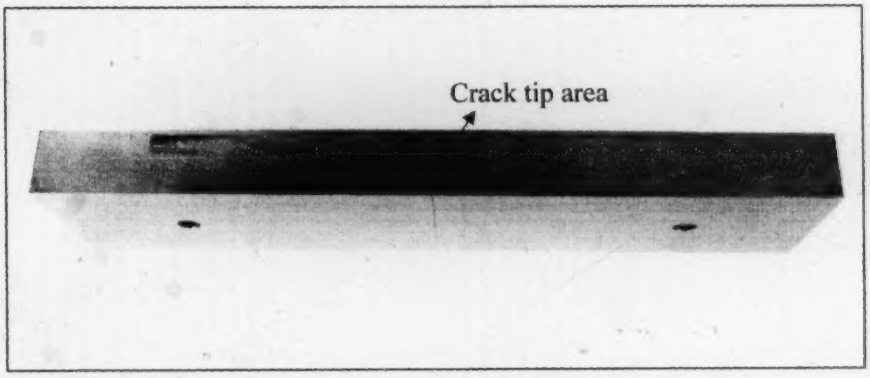

Figure 10: Specimen with removed notch. 2-drilled holes were made for loading with screws on the specimen jig

3.3 Analysis of Compliance Test Data

The value of crack opening load can be estimated by locating the point on the load-strain plot at which the curve becomes linear. Matlab is used to fit the linear line using the least-square fitting method by selecting the last data point as the origin and regressing backward toward zero. The initial trial uses 10 – 15 % of the last data points and a linear line is fitted to those data points. The number of data points that are used to fit the linear line is increased until the fitted line is no longer in alignment with the plotted compliance data. The best fit is estimated by visually observing the alignment between the fitted line and the plotted curve while monitoring the residual value of the least square method. The fitted straight line is found to be sufficient when its residual value is approximately 0.046. The data point at which this residual value is reached corresponds to the crack opening load. The load vs. displacement data from the compliance tests of specimen CO1, CO2, CO3 and CO4 are plotted in Figure 11, Figure 12, Figure

13 and Figure 14, respectively. The estimated crack opening loads for all specimens are shown in Table 3. Using the least square fitting method to determine the crack opening load on all specimens, it was found that crack opening load does not follow any trend in relation to crack depth.

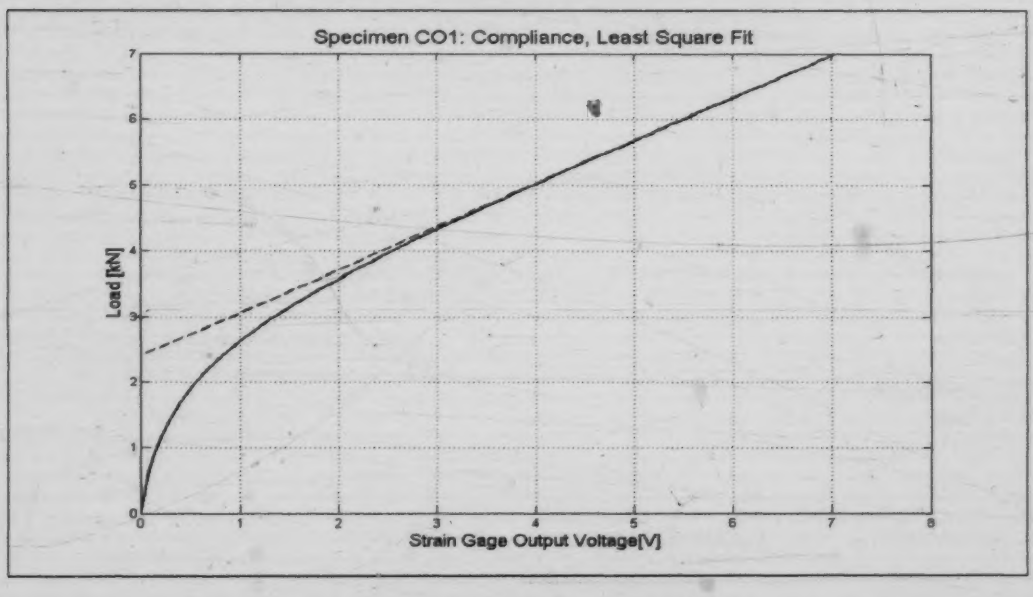

Figure 11: Compliance test of specimen CO1 (solid line = recorded data, dash line = fitted line)

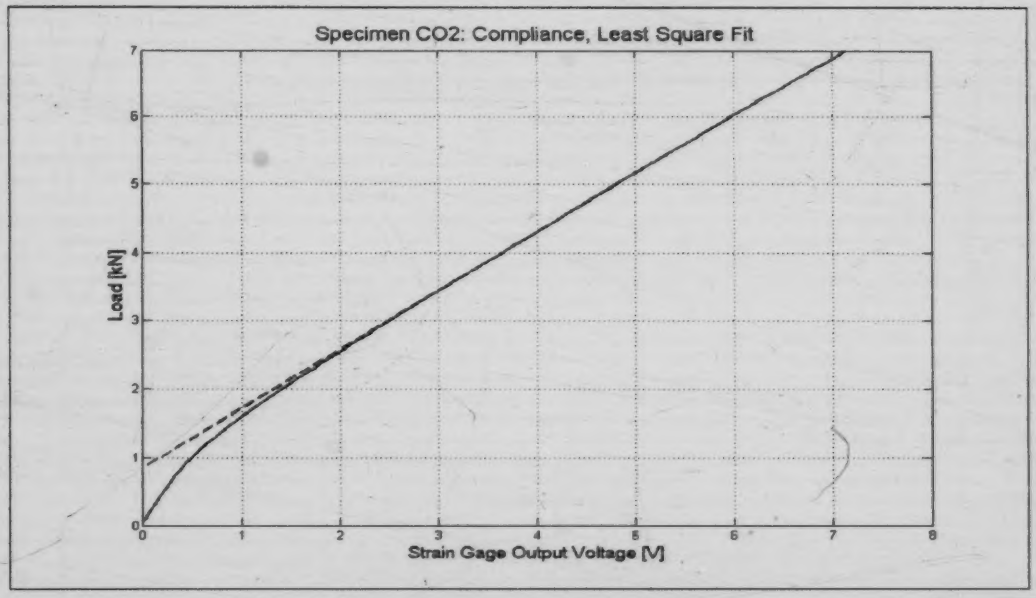

Figure 12: Compliance test of specimen CO2 (solid line = recorded data, dash line = fitted line)

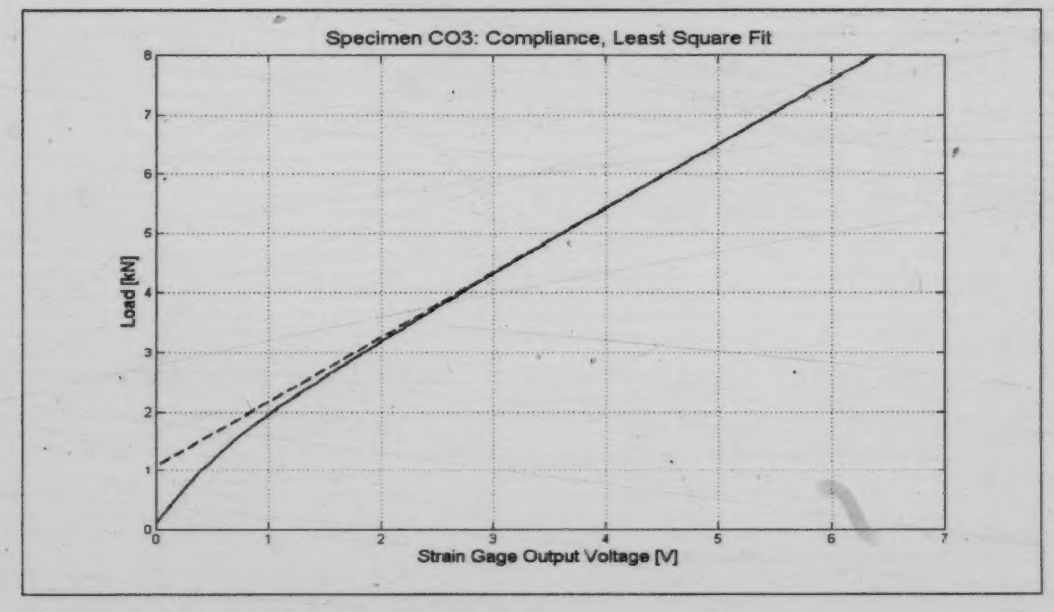

Figure 13: Compliance test of specimen CO3 (solid line = recorded data, dash line = fitted line)

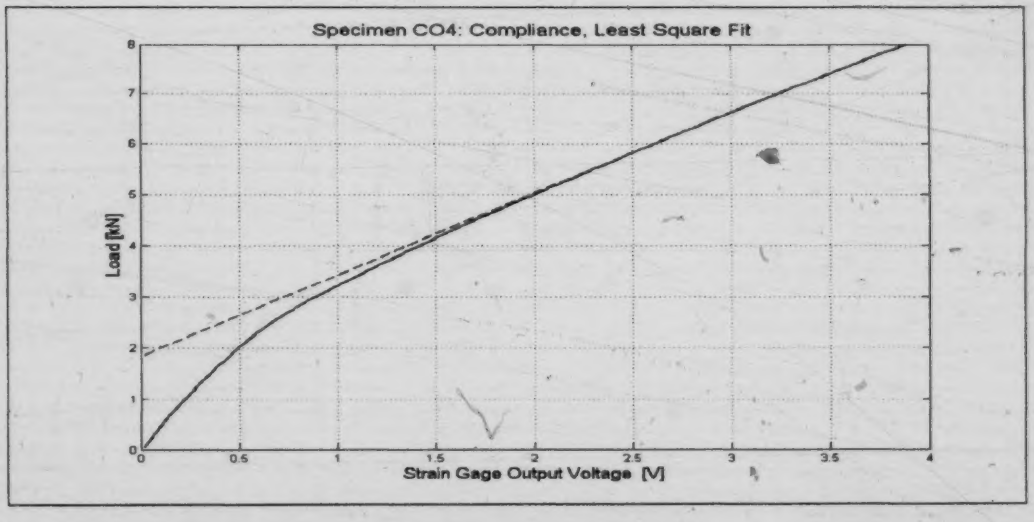

Figure 14: Compliance test of specimen CO4 (solid line = recorded data, dash line = fitted line)

Specimen	Opening Load [kN]
CO1	4.8964
CO2	3.5031
CO3	5.1723
CO4	5.6006

Table 3 Estimated opening load based on least-square method

In order to produce a more consistent measurement, the crack opening loads are also determined using ASTM E 647 "Recommended Practice for Determination of Fatigue Crack Opening Load from Compliance". This method utilizes the change in slope or inverse of compliance from the load – strain curve and the crack opening load is determined at a minimum of 2% slope offset. The calculation of the slope offset percentages is as follows. From the load-

displacement data, a linear line is fitted to approximately 25% of the last data points, as shown in Figure 15. The compliance value of this line is assumed to be the compliance of the fully open crack.

Then, the variations of compliance value with respect to different load levels are calculated by fitting straight lines to small overlapping segments of the load – displacement data. This small segment spans approximately 10% of the whole data. The compliance offset is formulated as:

$$Compliance\ offset = \frac{Small\ segment\ compliance - Open\ crack\ compliance}{Open\ crack\ compliance} \times 100\%$$

The load – compliance offset plots and table of crack opening load for each specimen are shown in the Figure 16 to Figure 19. From these figures, it can be seen that when the Load/Maximum Load ratio is approaching 1, the offset value of the small segment data is zero. The crack opening load is then determined as the lowest load where the compliance offset value is equal to 2% [19].

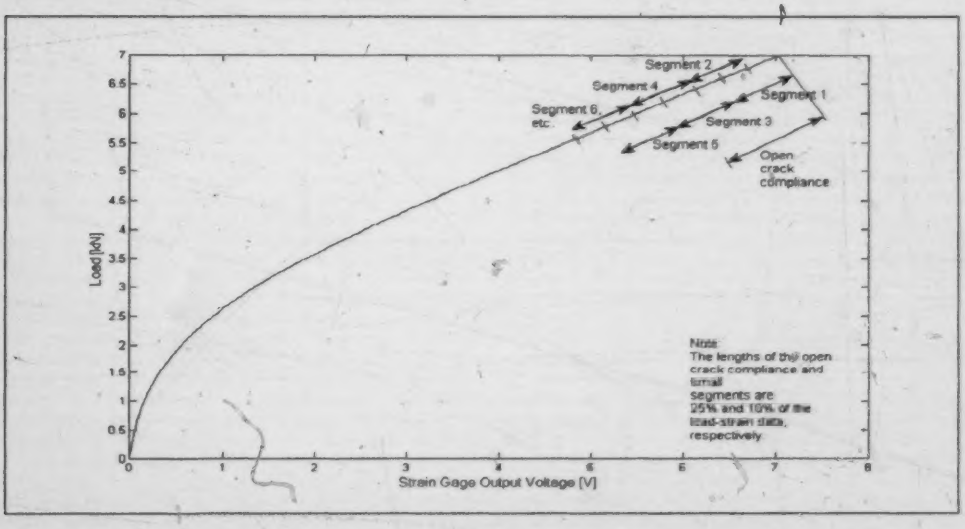

Figure 15: Variation of compliance with load to determine the crack opening load

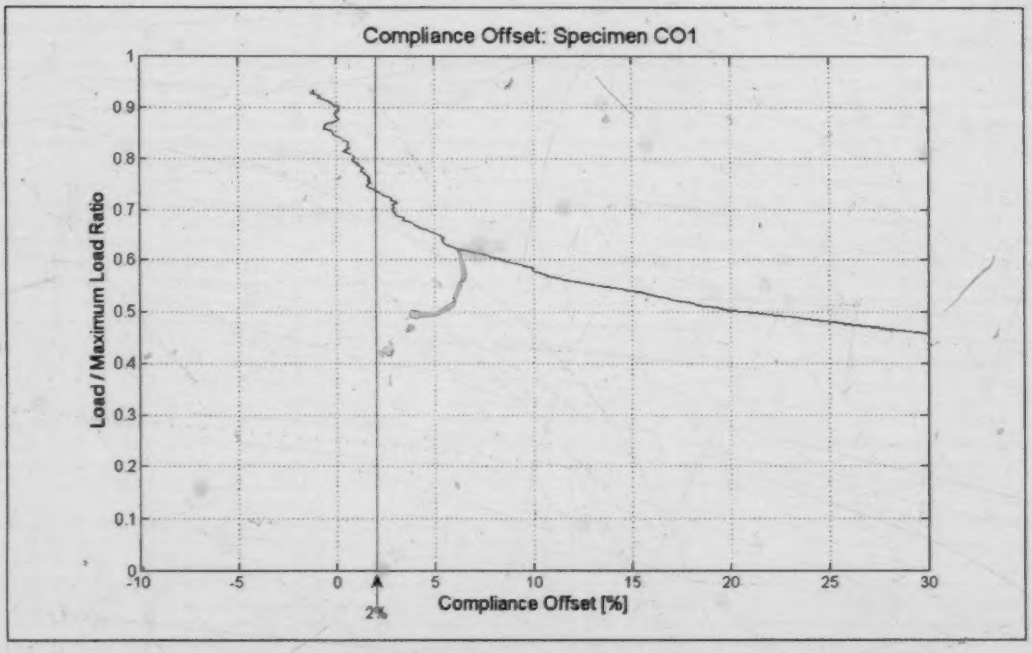

Figure 16: Compliance offset of specimen CO1 based on ASTM E 647

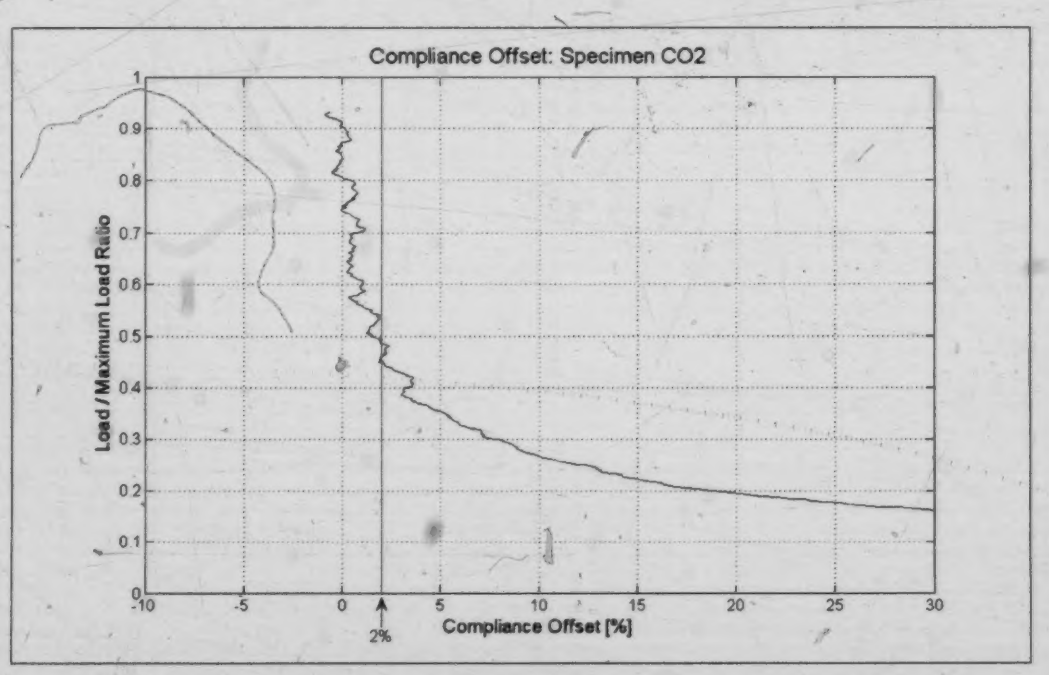

Figure 17: Compliance offset of specimen CO2 based on ASTM E 647

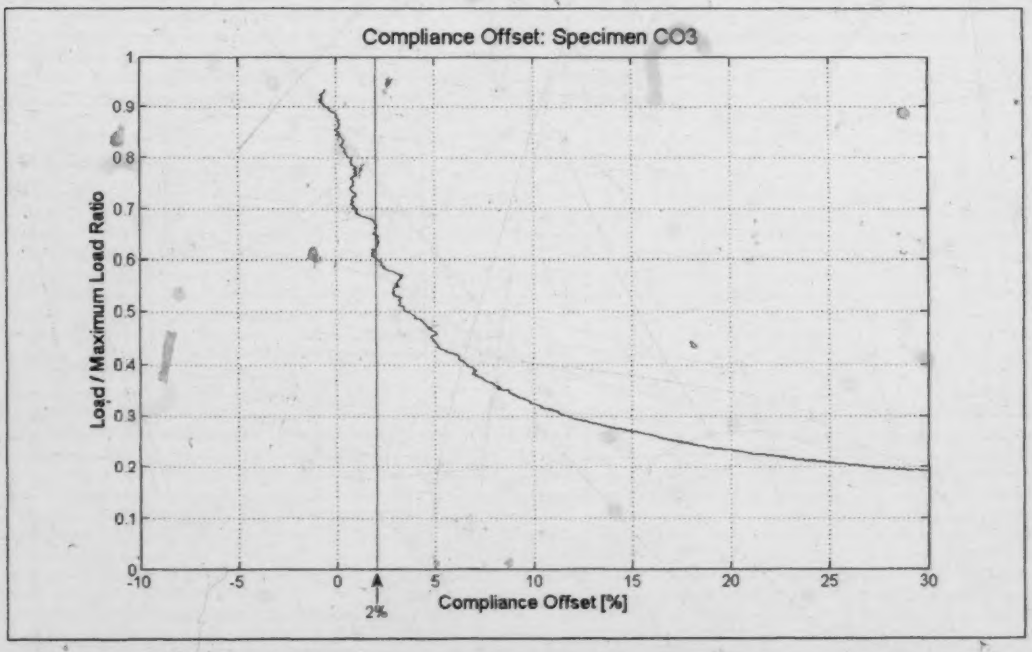

Figure 18: Compliance offset of specimen CO3 based on ASTM E 647

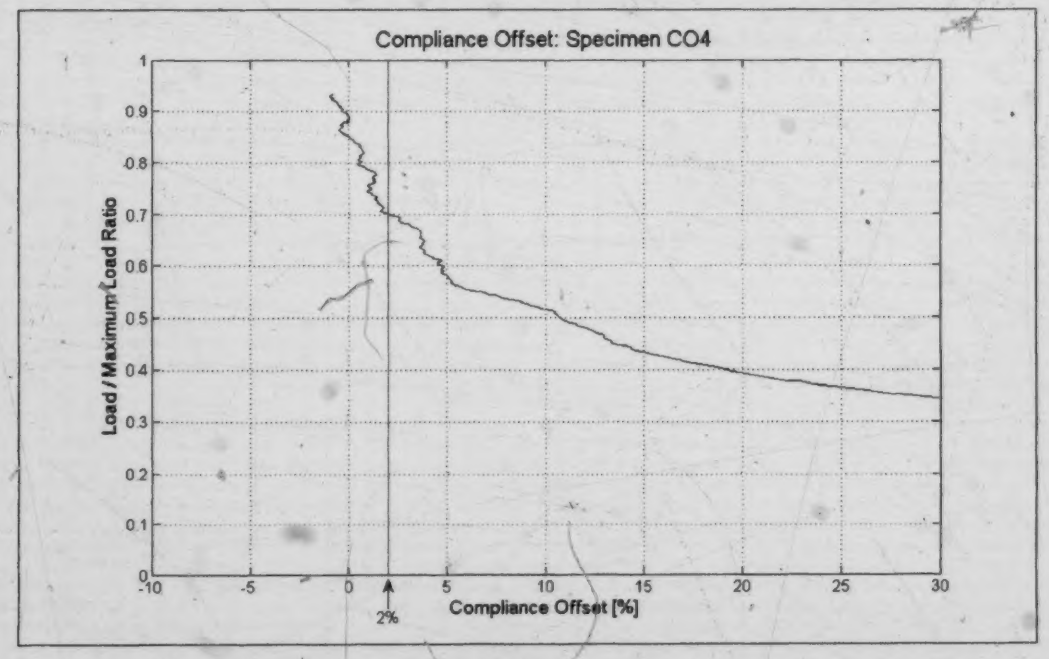

Figure 19: Compliance offset of specimen CO4 based on ASTM E 647

Keeping in mind that closing and opening stress will be introduced using the 4-point-bending specimen jig, it is necessary to know the load level at which each experiment is conducted. Using the specimen jig, the bending load is increased as the screws that go through the specimen are tightened into the jig. Positioning the steel rollers outside the screws will produce opening stress and placing them in between the screws will introduce closing stress to the crack surfaces. The jig setup that produces crack opening stress is depicted in Figure 20b. Note the positions of the screws that are in between the rollers.

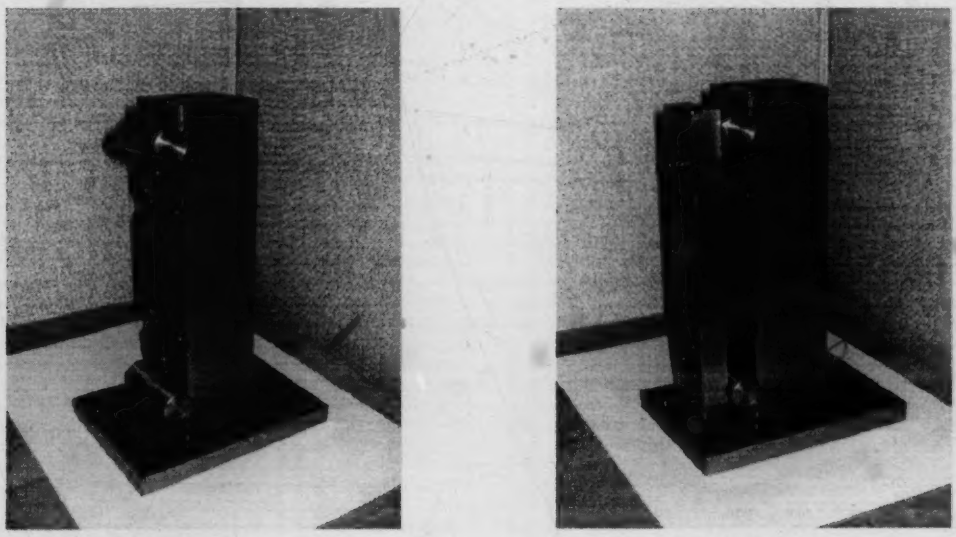

(a) (b)

Figure 20: Four-point-bending specimen jig without specimen (a) and with specimen (b)

In order to be able to accurately load the specimen using the fixture, two strain gages are placed 20 mm to the left and right side of the crack to monitor the manually applied load as shown in Figure 21. One can see that the application of

strain gages is different compared to those used in compliance testing. The main reason is the location of the strain gage relative to the mouth of the fatigue crack. In compliance testing, the strain gage is applied on the mouth of the starter notch and thus, the measured strain or opening on the fatigue crack mouth can be detected more sensitively. If the strain gage is to be applied in the same manner for load calibration, the measured strain will be very small because it is measured directly on the mouth of the fatigue crack. Thus, by attaching the strain gages on the left and right side of the crack, one will measure the strain experienced by the surface of the steel block and the load applied by turning both screws can be balanced with greater accuracy than using only one strain gage straddling the fatigue crack mouth opening.

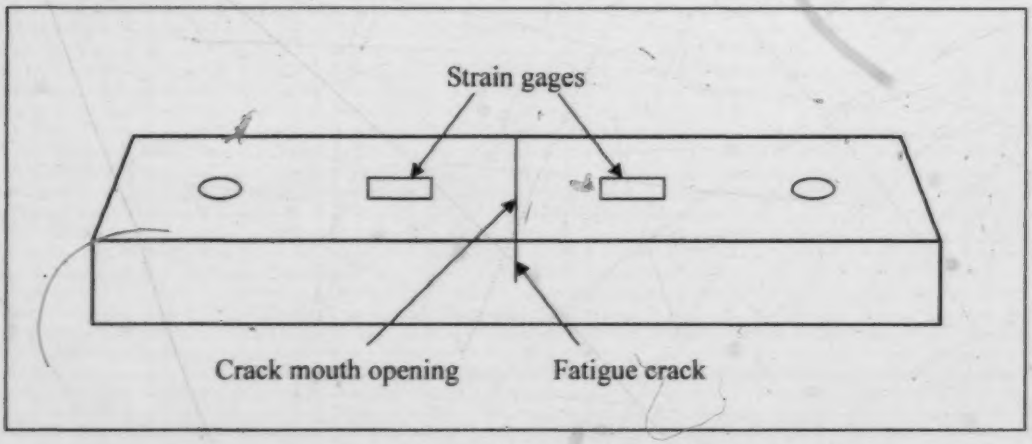

Figure 21: Strain gages on the left and right side of the crack

Load calibration for the strain gages is carried out by applying a monotonically increasing 4-point-bending load on each specimen using a fatigue testing (MTS) machine for both opening and closing stress and the resulting values of load vs. strains are plotted. Calibrating the strain gages is necessary to provide a

reference to produce the right amount of strains or load when applying the load manually during ultrasonic inspections on the specimen jig. Note that, a different loading machine is used because at this stage, the load is applied in a constantly increasing manner and hence, loading frequency does not play any role and it is not necessary to use the high frequency Vibrophore. The plots for load calibration data for all specimens are shown in Figure 22 to Figure 25.

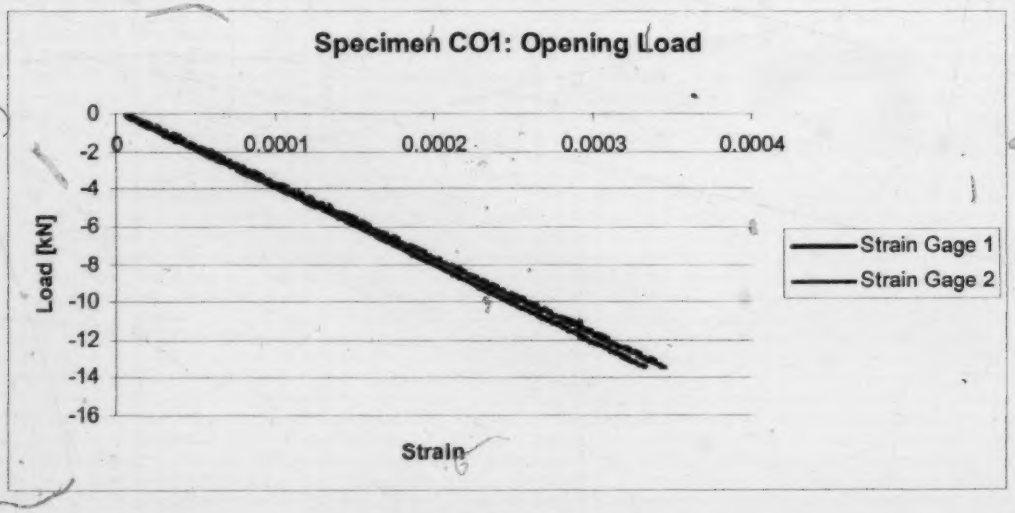

Figure 22 Load vs. strain plots of specimen CO1 under opening load on MTS machine

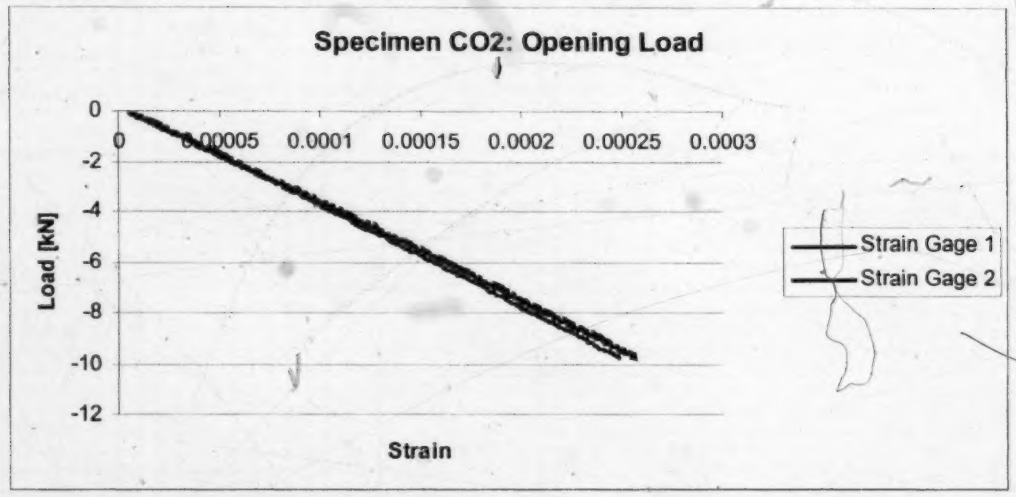

Figure 23 Load vs. strain plots of specimen CO2 under opening load on MTS machine

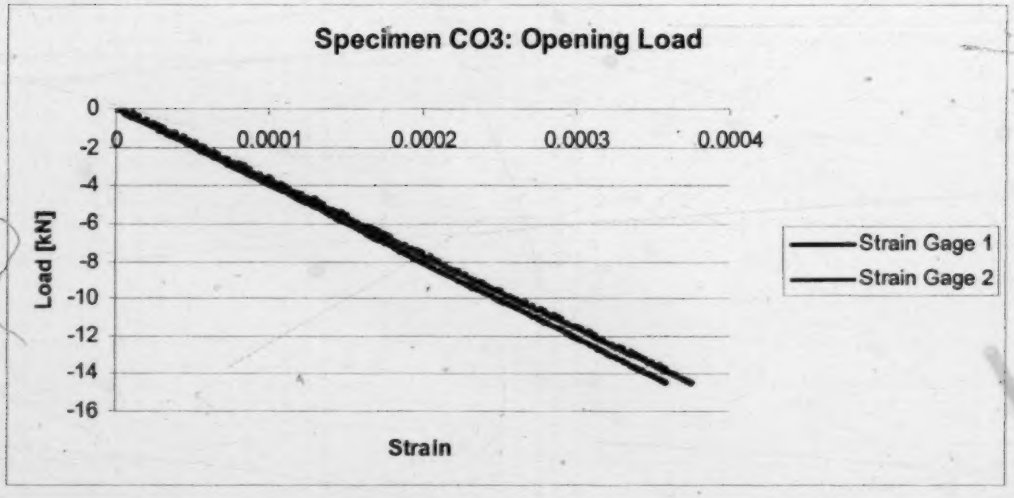

Figure 24 Load vs. strain plots of specimen CO3 under opening load on MTS machine

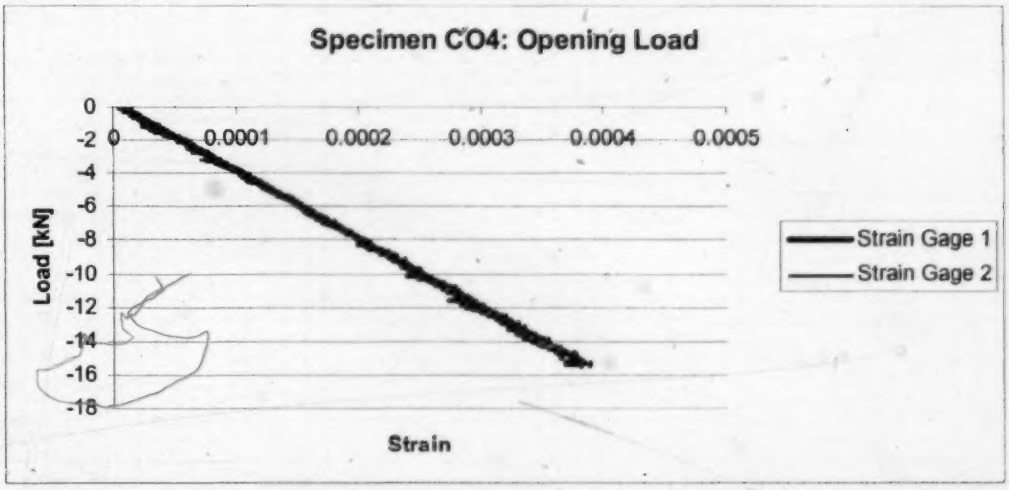

Figure 25 Load vs. strain plots of specimen CO4 under opening load on MTS machine

The load level introduced by the specimen jig shown in Figure 20 is estimated using a strain indicator. When connected to the strain gages, it measures the electrical current excited by each strain gage when the load is applied. Then, measured strains are compared with those obtained from the MTS machine to estimate the loading level. Note that, the strain indicator displays the strain value in mm/m and therefore, it is necessary to convert the strain unit recorded during load calibration. The conversion formula is [30] [44]:

$$\varepsilon_0 = \frac{1}{4} \cdot Ks \cdot \varepsilon \cdot E \qquad (6)$$

where:

ε_0 = output voltage of the strain gage [V]

Ks = gauge factor (2.145)

ε = actual strain

E = bridge voltage (5 V)

Rearranging the formula for calculating the actual strain:

$$\varepsilon = \frac{4 \cdot \varepsilon_0}{Ks \cdot E} \qquad (7)$$

Therefore, as the load applied manually on the specimen by tightening the screws, the strain value recorded by the strain indicator for each strain gage is compared to the actual strain value calculated using equation (7).

Chapter 4 Ultrasonic Testing

In this chapter, the methodology and results of the ultrasonic data analysis will be presented. The first step of the ultrasonic testing is obtaining data from specimens with artificial defects whose geometries are predetermined. Then, the collected ultrasonic data is used to estimate the size of those artificial defects. A novel crack size estimation method based on graphical solution is developed to improve the sizing accuracy of the existing method. Similar procedures are followed to evaluate the specimens with fatigue cracks and the corresponding results regarding the effect of fatigue crack surface contact on ultrasonic signal and improvement of sizing accuracy obtained by using the graphical solution are discussed.

4.1 Shear Wave Angle Beam with Contact Transducer

After all the specimens have been tested for its compliance and the corresponding crack opening loads have been determined, the specimens are ready to be inspected with ultrasonic nondestructive testing. The method of choice is angle beam shear wave with incident angle of 45^0. Angle beam shear wave is preferred to longitudinal wave because at the same frequency range, it is more sensitive to evaluate vertical crack. Furthermore, shear wave is preferred over longitudinal wave due to the small size of the fatigue cracks produced in the specimens.

Shear wave is generated into the specimen by means of Lucite wedge and this wedge will be directly in contact with the specimen surface. Angle of incidence of

45^0 is selected out of the available 45, 60 and 70-degrees wedges on the basis of experimental and theoretical results presented by Golan et al. [23] that angle beam reflection coming from vertical crack reaches its optimum amplitude when the incident angle ranges from 40 to 50^0. In their work on ultrasonic diffraction technique, it is found that for pitch-catch configuration, tip diffracted signal is optimum when the shear wave incident angle is 35^0. For pulse-echo configuration, 50^0-incident wave will produce the strongest tip signal. The use of 45^0 angle in our ultrasonic inspection of fatigue cracks is still justified as the amplitude of tip diffracted wave at this angle is equal for both pulse-echo and pitch-catch configurations. Also, the calculated amplitude is only slightly weaker than both 35^0 incident pitch-catch and 50^0 incident pulse-echo.

For every specimen, ultrasonic responses are collected under different load conditions. Since the crack opening load for each specimen is different, the inspection is conducted at 25% load increments of the full opening load. In addition to those, two sets of experiments at 5% and 10% above the full opening load are also carried out. The main purpose is to observe whether there is any significant changes when the specimen is loaded higher than the pre-determined opening load. If the amplitude change is prominent, that means the mathematically calculated crack opening load is inaccurate and adjustments need to be made on the mathematical parameters of the compliance offset method, such as the amount of data that is used as the open crack and small segment compliances. If there is no significant changes, that implies the capability and accuracy of ultrasonic nondestructive method for investigating

fatigue crack with its closure phenomenon. In the following section, the signal analysis of EDM specimens and fatigue cracks are presented. Also, signals originating from crack corner and crack tip will be treated separately as the experiments for each signals are conducted differently.

Crack feature extraction from the ultrasonic signal will be carried out based on amplitude of the first reflection from the corner of the fatigue crack and time-of-flights of the ultrasonic signal originating from both the corner and the tip of the fatigue crack. Amplitude of the ultrasonic signal will be plotted against its time-of-flight to produce an A-scan. There are two different ways to evaluate the amplitude of the collected ultrasonic signal. The first one utilizes the maximum value of the ultrasonic signal returning from the crack. This is done by applying full rectification on each A-scan data. By fully rectifying the ultrasonic signal, all the recorded amplitude will be converted to absolute values and thus, the peak of the ultrasonic signal will correspond to the absolute maximum point. Another method takes the whole amplitude range of an ultrasonic signal. This second method is called peak-to-peak method and it computes the amplitude difference between the maximum peak and the minimum peak of an ultrasonic signal. The schematic representation of both methods is shown in Figure 26. Plotting this maximum amplitude or peak-to-peak amplitude at each probe position will display the echo-dynamic corresponding to the inspected material and any existing flaw inside it.

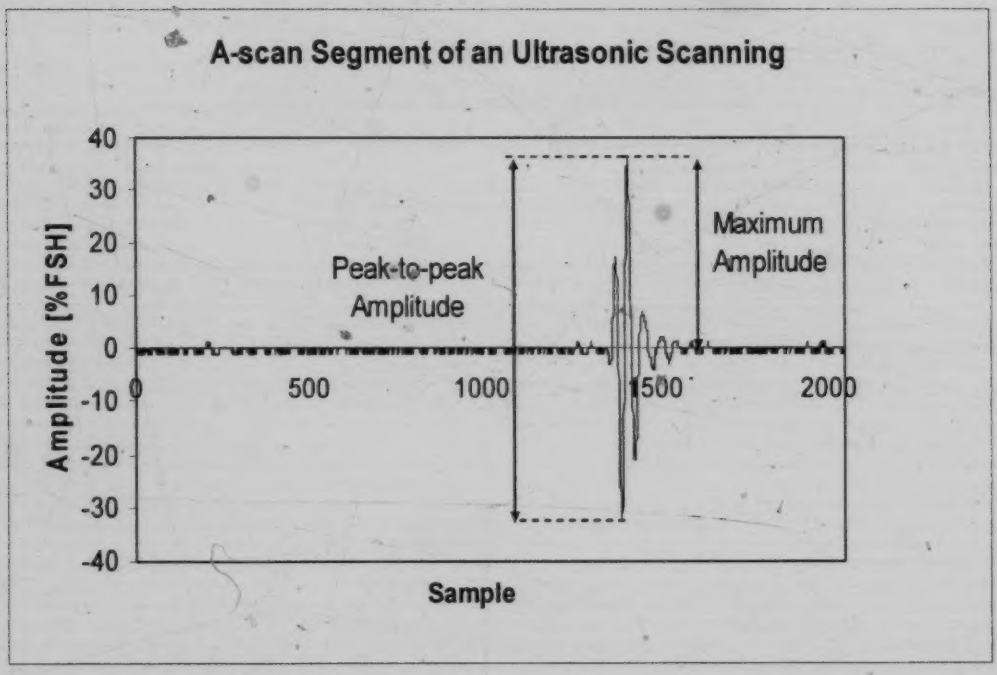

Figure 26: Feature extraction based on amplitude of an ultrasonic signal

On the other hand, crack identification and sizing with time-of-flight is not related to echo-dynamic because it linearly decreases as the distance between the probe and the crack reduces. The advantage of using time-of-flight over amplitude to measure a crack is that it can be used directly to compute the depth or location of the crack from single scanning. Inversely, amplitude-based crack sizing requires another group of ultrasonic signal collected from a specimen with known defect geometries for comparison.

4.2 Inspection on EDM Specimen

In order to provide the basis for crack measurement using ultrasonic signal amplitude, specimens with dimensions of 185 mm x 40 mm x 16 mm having

different depths of electro-discharge machined (EDM) slots were manufactured and inspected with the 45^0, 2.25 MHz angle beam contact transducer. The transducer is connected to a portable ultrasonic flaw detector, named Omniscan UT. The specimens analyzed have EDM slot depths varying from 0.5 mm to 3 mm with 0.5 mm increment and is fixed onto the specimen jig shown in Figure 20.

In order to achieve consistent transducer's movement and contact pressure onto the inspected specimen surface, the transducer is mounted onto a customized probe fixture which has 2 degree-of-freedom and the probe fixture is mounted onto a motorized linear scanner called BiSlide. The BiSlide system is programmed to move the transducer in a straight line starting from approximately 30 mm away from the crack to exactly above the crack location. For every probe movement of 0.25 mm, the BiSlide controller will send a pulse to the Omniscan UT to mark its location on the scan axis of the B-scan display. Scanning for each specimen is conducted three times in order to observe the variability of the recorded ultrasonic signal. Two amplification levels, i.e., gain levels, are used for each dataset. The first gain level is set at 25 dB. At this level, the ultrasonic signal reflected by the crack corner can be observed clearly while the ultrasonic signal diffracted by the crack tip has very low amplitude, approaching to that of the baseline noise. In order to enable a better observation of the crack tip signal, a higher gain level at 57.5 dB is used.

The scanning result of each dataset is in the form of B-scan representation. B-scan is a two dimensional representation of the ultrasonic scanning. One axis

typically corresponds to the travel time or time-of-flight of the ultrasonic signal. During the ultrasonic inspection with Omniscan UT, the time axes on the Omniscan UT display can be converted to show the corresponding distance of a reflector, e.g., cracks, from the transducer. The x-axis of the collected data, however, is stored in sample number. The other axis represents the position of the transducer along the scanning line. Thus, a B-scan is actually a compilation of A-scan data taken at various position of the ultrasonic transducer. An example of a B-scan display can be seen in Figure 27. The area enveloped by the white dash ellipse marks the appearance of ultrasonic signal reflected by the corner of a 2.5-mm-deep EDM slot. Moreover, it can be said that B-scan is simply a compilation of a series of A-scans. A-scan representation shows an ultrasonic signal recorded by a transducer at one position. It has two axes in which the x-axis represents the travel time of the ultrasonic signal and the y-axis displays the amplitude of the signal. An example of an A-scan is previously shown in Figure 26.

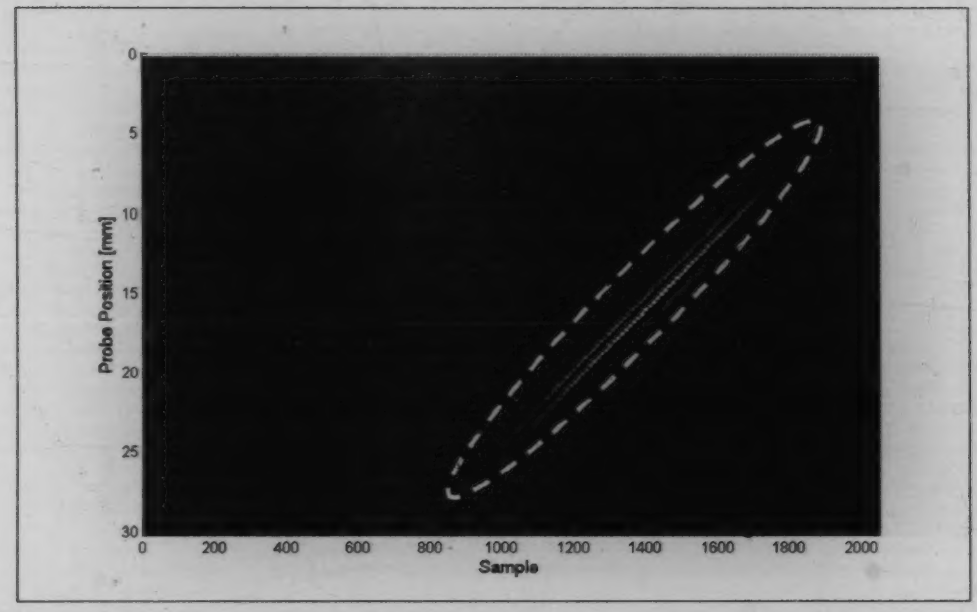

Figure 27: B-scan representation of ultrasonic signal amplitude from a 2.5-mm-deep EDM slot

4.2.1 Data analysis on crack corner signal

From the B-scan of each EDM specimens, the maximum fully rectified ultrasonic signal amplitude and the peak-to-peak amplitude at each probe position is recorded. The resulting plot will show the echo-dynamic of the ultrasonic signal as the transducer approaches and leaves the crack. An example of plotted ultrasonic signal amplitude originating from the slot corner of a specimen with 1.5 mm deep EDM slot is shown in Figure 28. It can be seen that ultrasonic nondestructive evaluation of materials is a repeatable technique. Among three data sets, there is only minimal difference of the recorded ultrasonic signal amplitudes. Also, ultrasonic signal amplitude is found to be sensitive toward the

change in EDM slot depths. After all the EDM specimens are inspected, the ultrasonic signal amplitude from the slot corners are extracted with fully rectified amplitude and peak-to-peak method and the resulting plots are presented in Figure 29 and Figure 30, respectively.

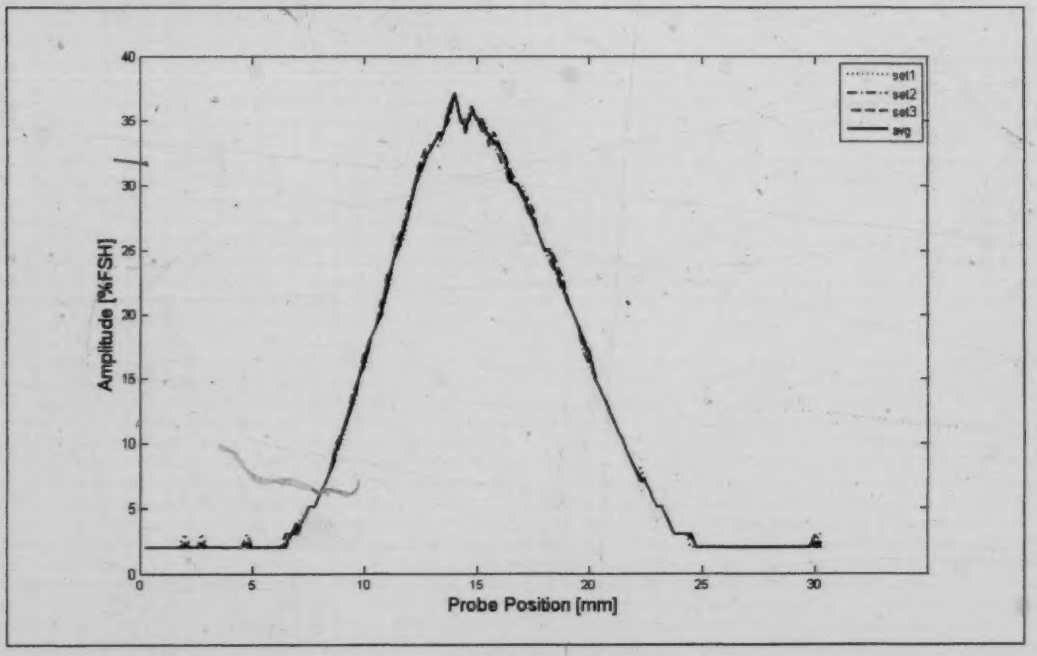

Figure 28: Echo-dynamics of the fully rectified ultrasonic signal amplitudes from the slot corner of specimen with 1.5-mm-deep EDM slot

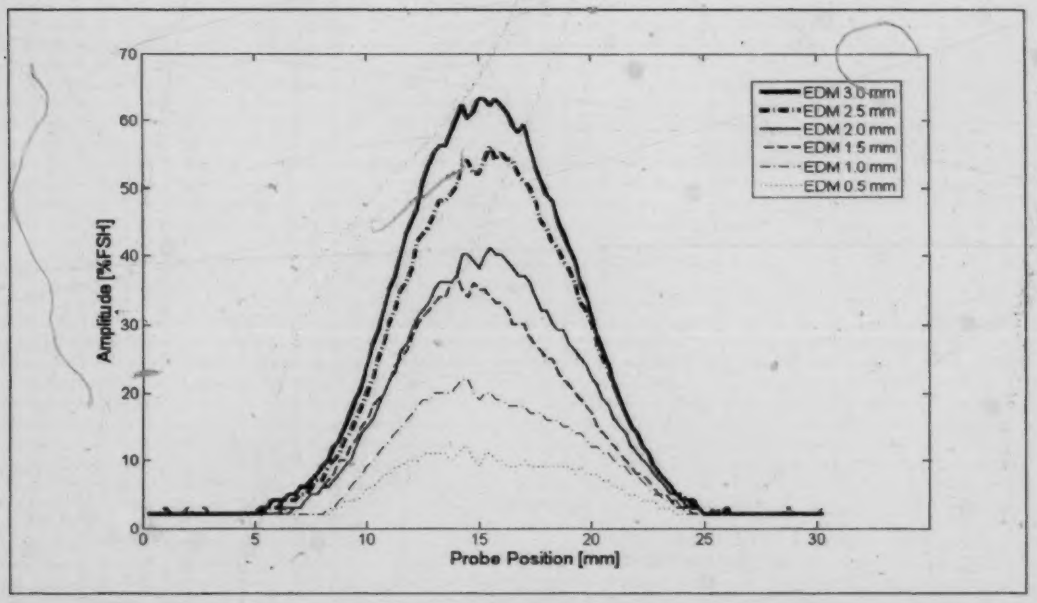

Figure 29: Echo-dynamics of the fully rectified ultrasonic amplitude of the slot corner of EDM slots with different depths

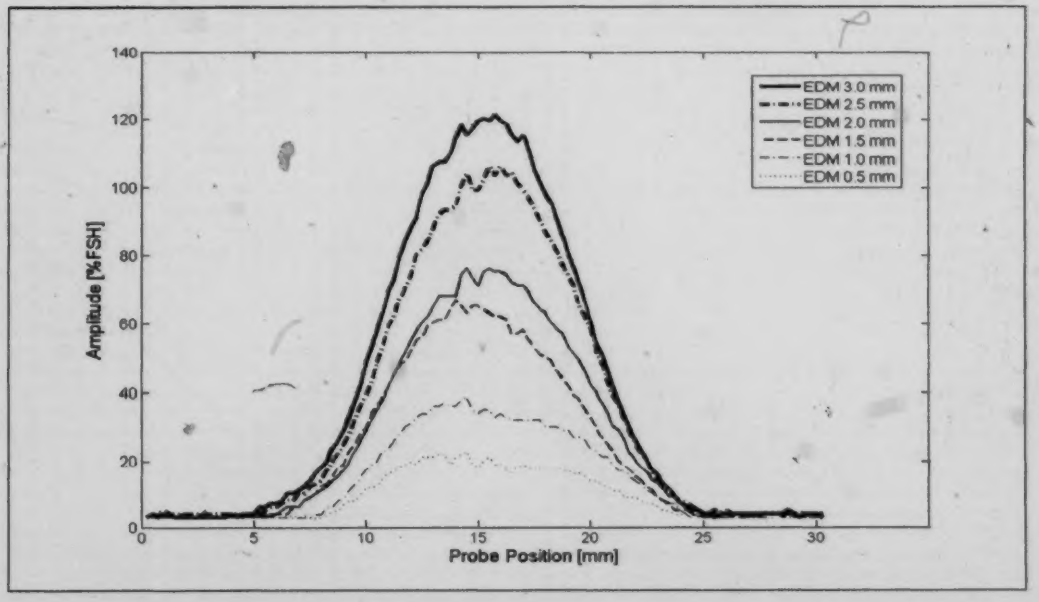

Figure 30: Echo-dynamics of the peak-to-peak ultrasonic signal amplitude of the slot corner of EDM slots with different depths

Both the maximum amplitude and the peak-to-peak method display a qualitatively identical trend between the ultrasonic signal amplitude and the depth of EDM slot. As the depth of the EDM slot increases, the amplitude of the ultrasonic signals increases when the ultrasonic transducer is at the vicinity of the crack. However, further observation shows that the echo-dynamic of the ultrasonic signal becomes more visible when the peak-to-peak amplitude, rather than only the maximum value, of an ultrasonic signal originating from the crack is used. Comparing the maximum amplitude and peak-to-peak amplitude of each EDM specimens, the sensitivity of peak-to-peak method is almost doubled compared to that of maximum fully rectified amplitude. From the extracted fully rectified amplitude and peak-to-peak amplitude, the maximum values from each specimen are selected to form the plot shown in Figure 31.

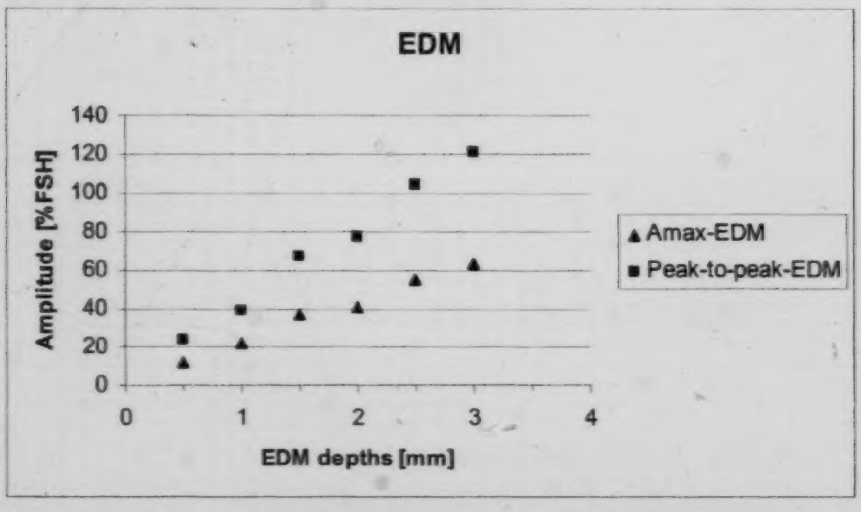

Figure 31: Peak values of ultrasonic signal amplitude from the corner of EDM slots with different depths

These peak values correspond to the probe position at which the centre beam from the transducer's crystal comes into contact with the corner of the EDM slot. Note that, during EDM process, the specimens do not experience any mechanical loading. Therefore, every EDM slot can be treated as a fully open crack and the ultrasonic signal amplitude collected from such an artificial defect can be used as the basis for size measurement of a fully open fatigue crack.

4.2.2 Data analysis on crack tip signal

As mentioned before, the observation of crack tip signal requires a high level of signal amplification, i.e., 57.5 dB. At this gain level, the ultrasonic signal diffracted by the crack tip is greatly amplified. However, noise level is also amplified making the identification of crack tip signal from the noise from an A-scan difficult. Note that, the crack corner signal is amplified as well such that it saturates and the peak point of the crack corner signal can not be observed. This is where the B-scan representation becomes useful. Since the B-scan shows the movement of the ultrasonic signal as the transducer's position changes, the crack tip signal can be observed more clearly. By locating the coordinate of a tip diffracted signal in a B-scan, i.e. probe position and sample number, using a grid, one can track the ultrasonic signal diffracted by the crack tip and record its corresponding amplitude and/or time-of-flight for all probe positions. B-scan display recorded at 57.5 dB gain and the same B-scan display with a grid are shown in Figure 32 and Figure 33, respectively. The solid and dash ellipses represent the crack tip signal and the saturated crack corner signal. The rectangle shows the appearance of

standing noise at this gain level. This standing noise originates from the angle beam wedge and is stationary along the time axis. It is usually not visible at low gain level. From Figure 33, when the transducer has traveled for 20 mm, a positive peak value of the ultrasonic signal diffracted from the crack tip can be observed at approximately sample number 1100. The A-scan display at this probe position is shown in Figure 34.

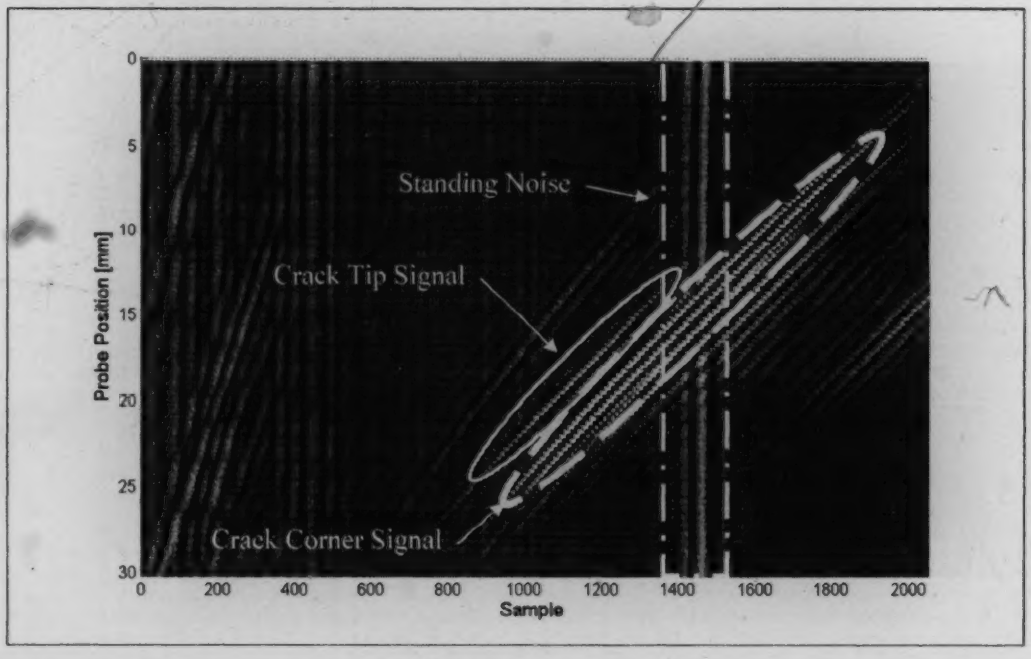

Figure 32: B-scan result of an EDM specimen with 3.0 mm slot depth at 57.5 dB gain level

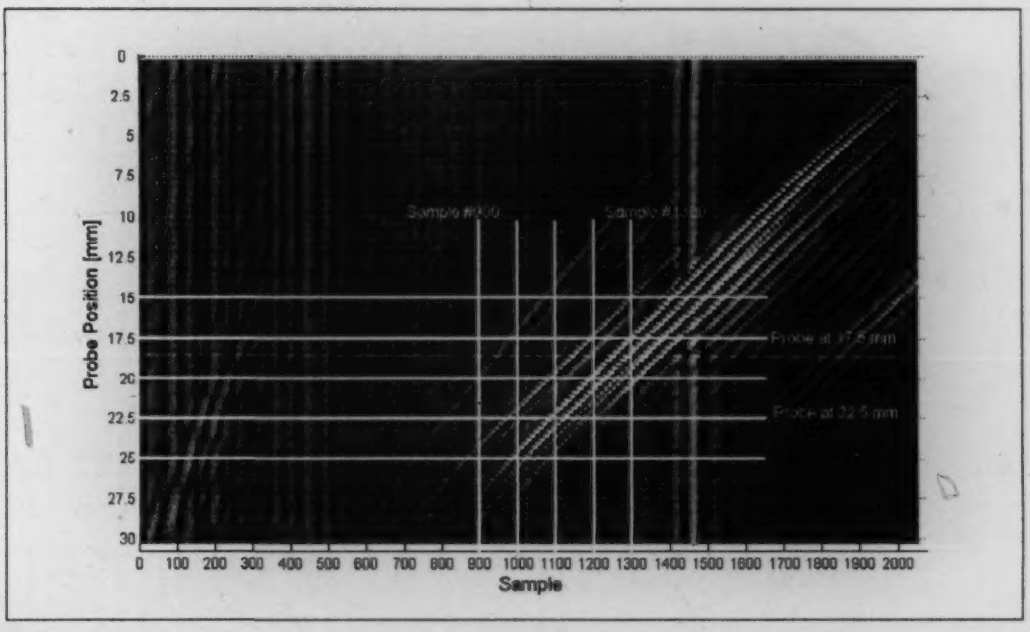

Figure 33: B-scan result of an EDM specimen with 3.0 mm slot depth at 57.5 dB gain level with grid

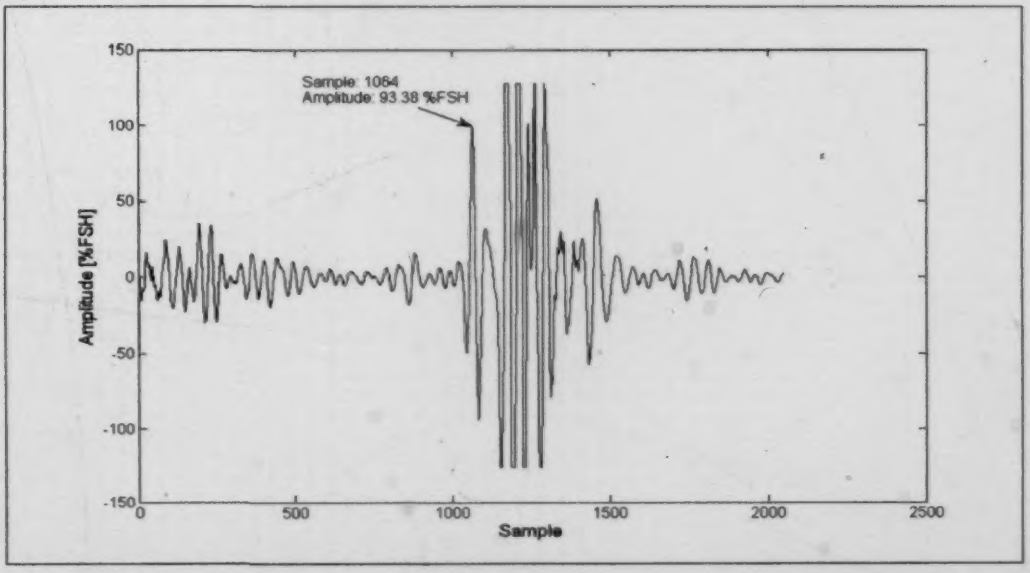

Figure 34: A-scan display of the ultrasonic signal collected from specimen with 3.0 mm deep EDM slot at the transducer's position of 20 mm.

It is necessary to check the A-scan at every probe position with B-scan as the guide to distinguish the crack tip signal from other signals including the noise so that the amplitude values at each probe position can be recorded. The resulting plots displaying the echo-dynamics of the ultrasonic signal diffracted from the crack tip for specimens with EDM slot depths from 1.5 mm to 3.0 mm are shown in Figure 35 to Figure 38. The echo-dynamics from specimen with EDM depths ranging from 0.1 to 1.0 mm can not be produced because the crack diffracted signal is overwhelmed by the ultrasonic signal from the crack corner and thus, can not be distinguished clearly.

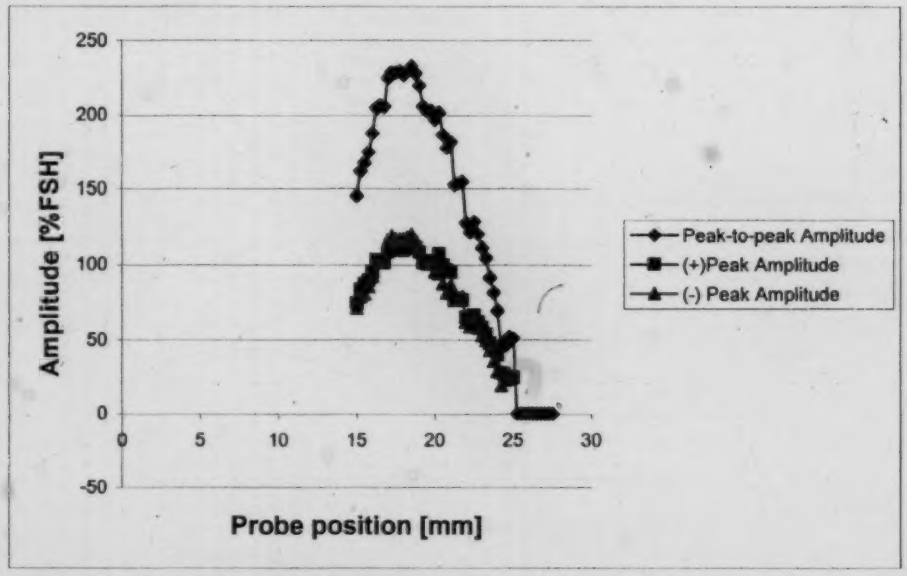

Figure 35: Echo-dynamics of ultrasonic signal diffracted from the crack tip of specimen with 3.0 mm deep EDM slot

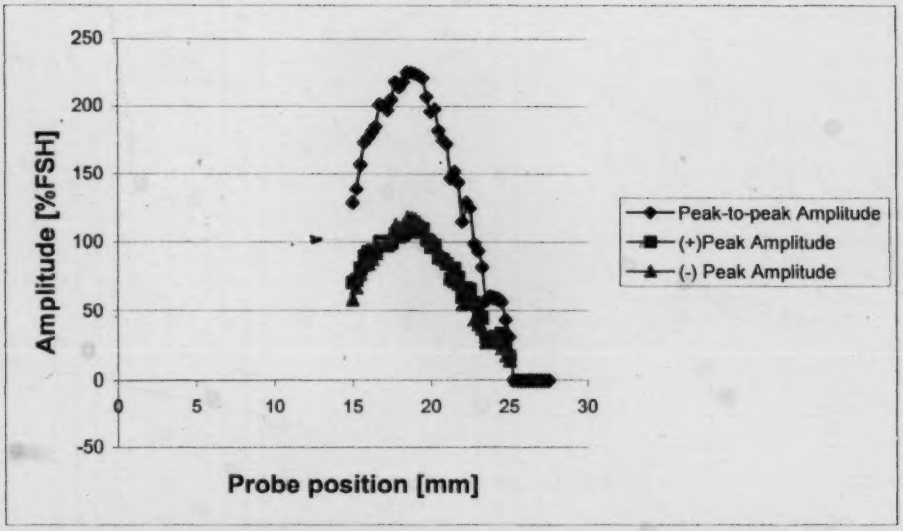

Figure 36: Echo-dynamics of ultrasonic signal diffracted from the crack tip of specimen with 2.5 mm deep EDM slot

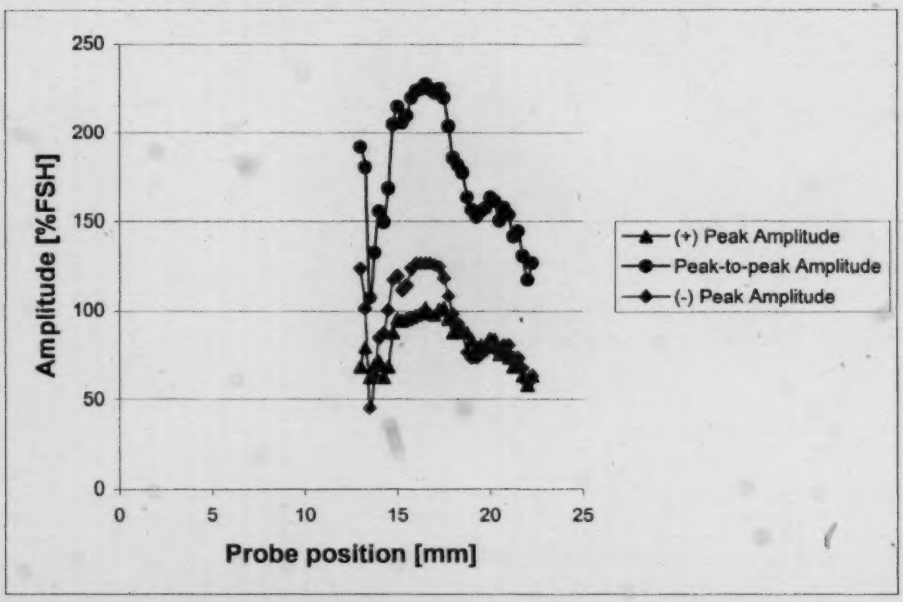

Figure 37: Echo-dynamics of ultrasonic signal diffracted from the crack tip of specimen with 2.0 mm deep EDM slot

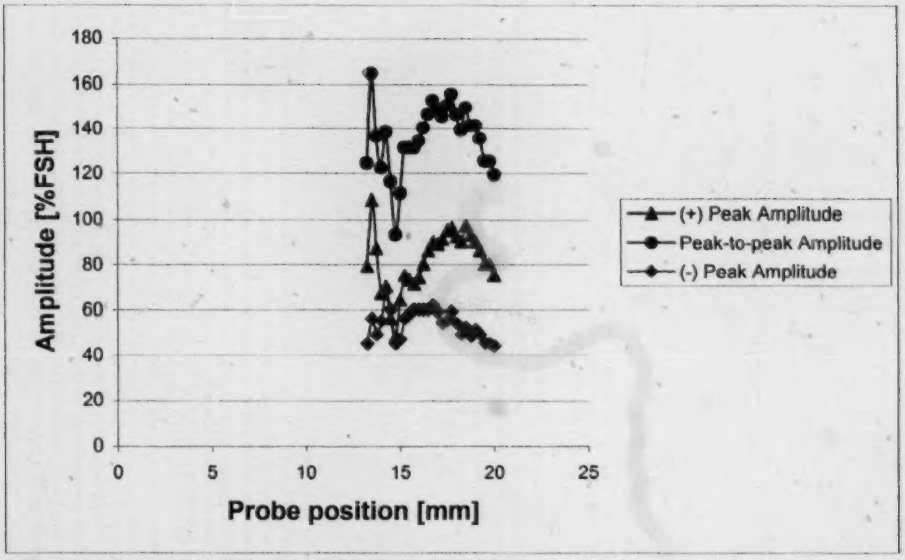

Figure 38: Echo-dynamics of ultrasonic signal diffracted from the crack tip of specimen with 1.5 mm deep EDM slot

By comparing the echo-dynamics of the tip diffracted ultrasonic signal from specimens with EDM slot depth from 2.0 to 3.0 mm, it can be seen that amplitude of the crack tips signal may not be the suitable parameter to differentiate crack depth because the peak amplitudes of the crack tip diffracted signal are almost identical for EDM slot depths of 2.0, 2.5 and 3.0 mm. Therefore, in order to analyze the crack tip data, the time of flight is used. Note that, the Omniscan UT is capable to convert the x-axis from time-of-flight to distance of wave propagation to the depth of a reflector from the scanning surface. In this experiment, the total number of samples or data points for every A-scan is 2048 and this is equal to a total time of 20.48 μs because the sampling frequency is 100 MHz. By incorporating the specifications of the transducer into the Omniscan UT, the time axis of 20.48 μs (or sample axis of 2048 data points) is calibrated

and the corresponding depth value is 23.46 mm. Therefore, using the sample number of the crack tip and crack corner signals, the crack depth can be estimated directly by scaling. If the sample number of the tip diffracted signal with maximum amplitude is n, then the corresponding distance of the crack tip location measured from the scanning surface of $n \times \frac{23.46\,mm}{2048}$. By subtracting this value from the measured specimen thickness, one will obtain the depth of the fatigue crack. The estimated crack depths for EDM specimens with slot depths from 1.5 mm to 3.0 mm are shown in Table 4.

EDM Slot Depth [mm]	Sample Number	Tip Position from the Scanning Surface [mm]	Estimated EDM Slot Depth [mm]	% Error
1.5	1225	14.03	1.97	31.33
2.0	1275	14.61	1.39	-30.5
2.5	1159	13.28	2.72	8.88
3.0	1131	12.96	3.04	1.33

Table 4: Estimated EDM depth using the calibrated axis of Omniscan UT

From Table 4, it can be seen that specimen with EDM depth of 3.0 mm is the specimen whose depth is estimated with the least error while specimens with EDM depths of 1.5 mm and 2.0 mm is oversized and undersized by great margins. In order to improve the accuracy of crack depth estimation, a solution based on graphical representation of the ultrasonic inspection with angle beam transducer is used. The schematic of this solution is shown in Figure 39.

The idea behind the graphical solution lies in the advantage of time-of-flight as the main parameter for calculating the traveling distance of the ultrasonic signal. The radius of the half-circles represents the length of the wave propagation path between the reflector, i.e., crack tip or crack corner, and the transducer's beam index point. The first half-circle marks the location of the transducer relative to the location of the crack corner and the second one indicates the location of the transducer relative to the location of the crack tip. In this method, the propagation angle of the maximum amplitude of the ultrasonic signal reflected from the corner of the crack depends on the transducer angle. This is basically the refraction angle due to the wedge of the angle beam transducer. In our case, this angle is 45^0.

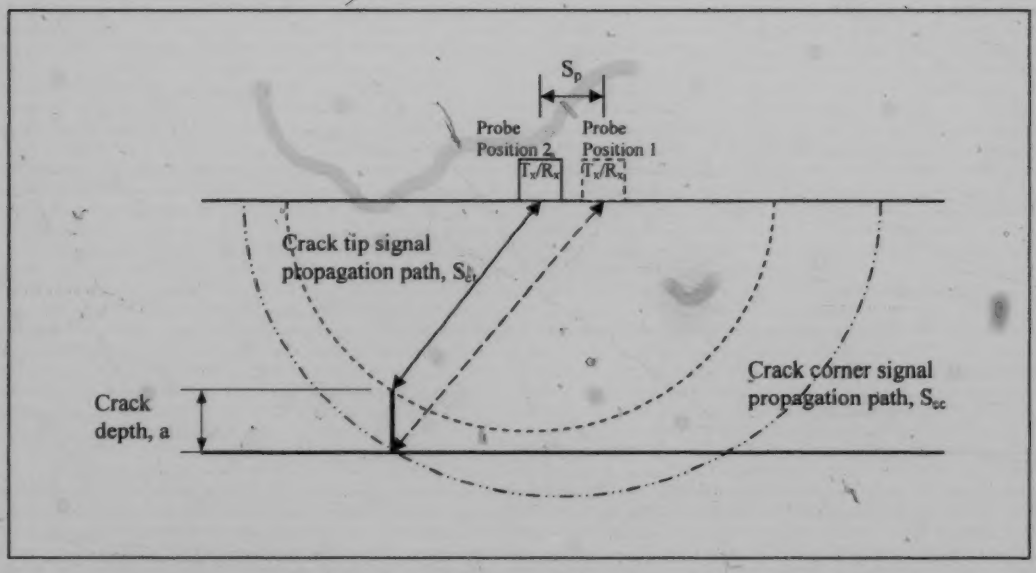

Figure 39: Graphical representation of the solution for crack depth estimation

On the other hand, ultrasonic wave due to diffraction propagates in all directions. Therefore, for this graphical solution, the diffracted angle that yields the maximum amplitude of crack tip diffracted signal is not fixed and remains as a variable. Knowing the transducer's positions and sample number, i.e., time-of-flight, that yield maximum amplitudes of ultrasonic signal reflected by the corner of the crack and diffracted by the crack tip, the crack depth can be estimated using Figure 39 to obtain the following equations:

$$S_{cc} = n_{cc} \times v \times 10^{-5}$$

$$S_{ct} = n_{ct} \times v \times 10^{-5}$$

$$a = \frac{S_{cc} \times Sin45^0}{2} - \left[\left(\frac{S_{ct}}{2} \right)^2 - \left\{ \frac{S_{cc} \times Sin45^0}{2} - S_p \right\}^2 \right]^{\frac{1}{2}}$$

where:

n_{cc}: Sample number of the crack corner signal

n_{ct}: Sample number of the crack tip signal

S_{cc} : Length of ultrasonic wave propagation for the crack corner signal

S_{ct}: Length of ultrasonic wave propagation path for the crack tip signal

S_p: Distance between probe position 1 (crack tip signal with maximum amplitude) and probe position 2 (crack corner signal with maximum amplitude)

a: crack depth

Using this equation, the depths of the EDM slots are estimated by taking not only the parameters of the ultrasonic signal with maximum amplitude, but also the existing neighboring peak values. In Figure 35 to Figure 38, it can be seen that

other than the probe position with maximum amplitude value, there exist several points whose amplitudes are comparable to that of the maximum value. It is suspected that these peaks occur due to the surface roughness around the edge of the EDM slot whose effect is not as obvious in the larger slot. Moreover, other peak points can be observed in Figure 37 and Figure 38. These peak points are tested on the graphical solution as well. There are 3 datasets for each ultrasonic inspection at a gain level of 25 dB or 57.5 dB. The EDM slot depths are estimated by randomly pairing these datasets, e.g., for specimen with EDM slot depths of 2.5 mm, dataset 1 of 25 dB is paired with dataset 2 of 57.5 dB. The resulting EDM slot depths for each EDM specimen is summarized in Table 5.

EDM Slot Depths [mm]	Dataset # at 25 dB	Dataset # at 57.5 dB	Estimated EDM Slot Depths [mm]	%Error
1.5	2	2	1.558	3.87
2.0	2	1	2.1571	7.86
2.5	3	3	2.7124	8.5
3.0	1	3	3.2139	7.13

Table 5: Estimated EDM depths based on graphical solution

From Table 5, it can be seen that the graphical solution provides more consistent estimation of the EDM slot depths using time-of-flight of the ultrasonic signal diffracted from the crack tip and reflected from the crack corner. Therefore, the graphical solution will be used as the crack depth estimation method for the fatigue crack specimens.

4.3 Inspection on Fatigue Crack Specimen

Following the ultrasonic inspection of EDM specimen, the fatigue crack specimens with dimensions of 185 mm x 40 mm x 16 mm with four different fatigue crack depths is inspected using the 45^0, 2.25 MHz angle beam contact transducer. The transducer is connected to a portable ultrasonic flaw detector, named Omniscan UT. Similar to the EDM specimens, every fatigue crack specimen is inspected starting from approximately 30 mm away from the crack with a scanning step size of 0.25 mm and sampling frequency of 100 MHz. Two amplification levels, i.e., 25 dB and 57.5 dB that are used for ultrasonic inspection of EDM specimens are utilized to evaluate the fatigue crack specimens. Scanning for each specimen is conducted three times in order to observe the variability of the recorded ultrasonic signal. For each dataset, a B-scan representation is generated and each B-scan is composed of 120 lines of A-scans. Each A-scan corresponds to the collected ultrasonic signal at one probe position.

On the inspection of fatigue cracks, the ultrasonic signal is transmitted to the specimens at two different amplification levels. Both amplification levels are selected on the basis of round robin trials on specimen with largest crack depth. During the trials, ultrasonic data is collected at various amplification levels from 20 dB to 60 dB and two levels of signal amplification are selected to focus on crack corner and crack tip separately. After fixing a specimen onto the specimen jig and tightening the screws to produce fully open crack condition, the specimen is scanned at various gain levels from 20 dB to 50 dB. At the gain level of 25 dB,

it is found that for a 16-mm-thick steel plate specimen, the collected ultrasonic signal from the fatigue crack corner is sufficiently strong. Moreover, increasing the amplifier gain level larger than 25 dB will lead to a clipped/cut-off corner signal which will make peak amplitude selection impossible. On the other hand, higher amplification level of 57.5 dB is used to capture the crack tip signal. This level is selected with a trade-off between tip signal visibility and noise level. The specimens are numbered starting from the largest crack depth.

4.3.1 Data analysis on crack corner signal at varied load from no load to maximum opening load

As mentioned in the previous section, three datasets are recorded for each specimen under every loading level.

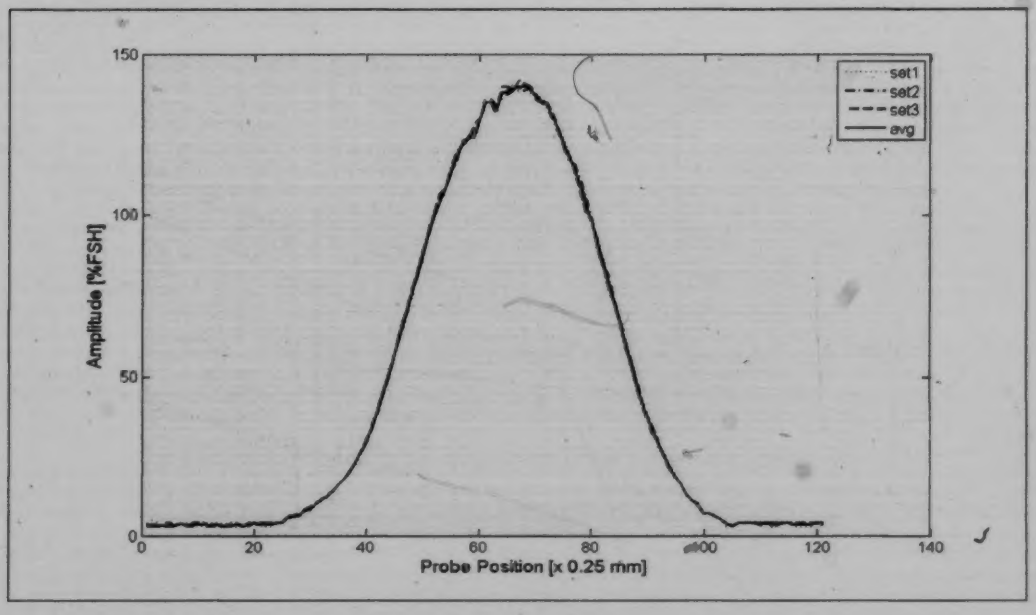

Figure 40: Extracted amplitude from specimen CO2 at 50% crack opening load

A sample of the echo-dynamics of the recorded ultrasonic signal originating from the corner of the fatigue crack is shown in Figure 40. It can be seen that the probe location at which corner signal reaches its maximum value can be determined. Also, three data sets taken at each loading condition are consistent. Although the load applied to the specimen remains constant for a particular loading condition, e.g., 50% crack opening load, the ultrasonic inspection condition may vary because the couplant is applied manually and thus, its amount may differ slightly among datasets. However, it can be seen that the difference in echo-dynamics between each data set is minimal and therefore, the ultrasonic nondestructive method is repeatable on fatigue cracks.

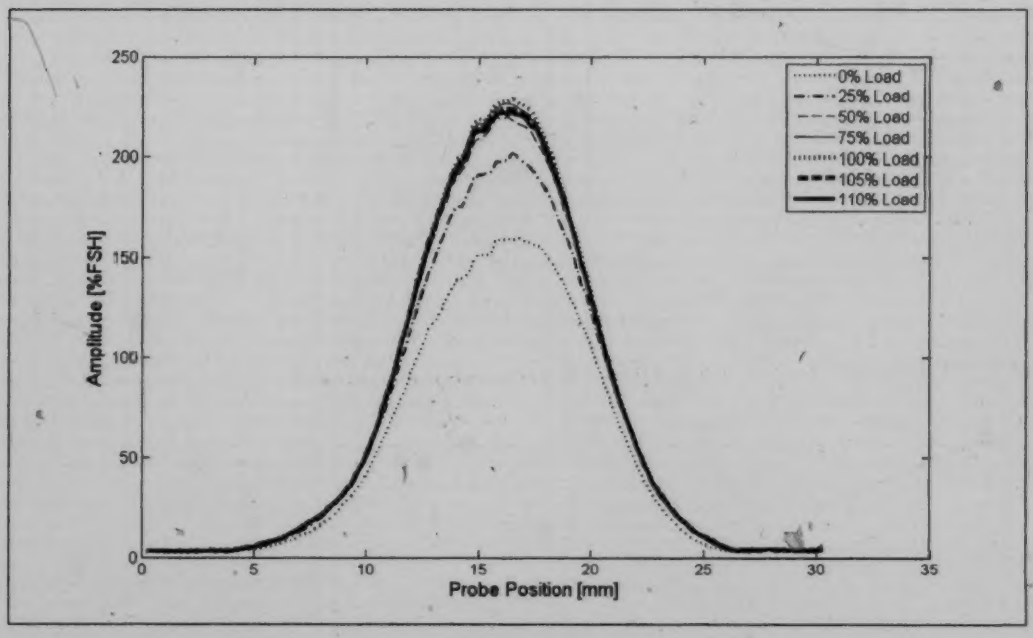

Figure 41: Extracted peak-to-peak amplitude from specimen CO1 at various crack opening loads

From Figure 41, it can be seen that the crack amplitude rises as the load is increased. It shows that the crack is partially closed when it is unloaded and as increase in amplitude of corner reflection can be related to increase of reflection surface which in this case is the crack surface. Also, it can be seen that increasing the loading level from 75% to 100% does not change the amplitude significantly and this shows that crack opening load is reaching its maximum value. This is further supported by the approximately similar amplitude levels when the specimen is loaded above the fully opening load by 5% and 10 %.

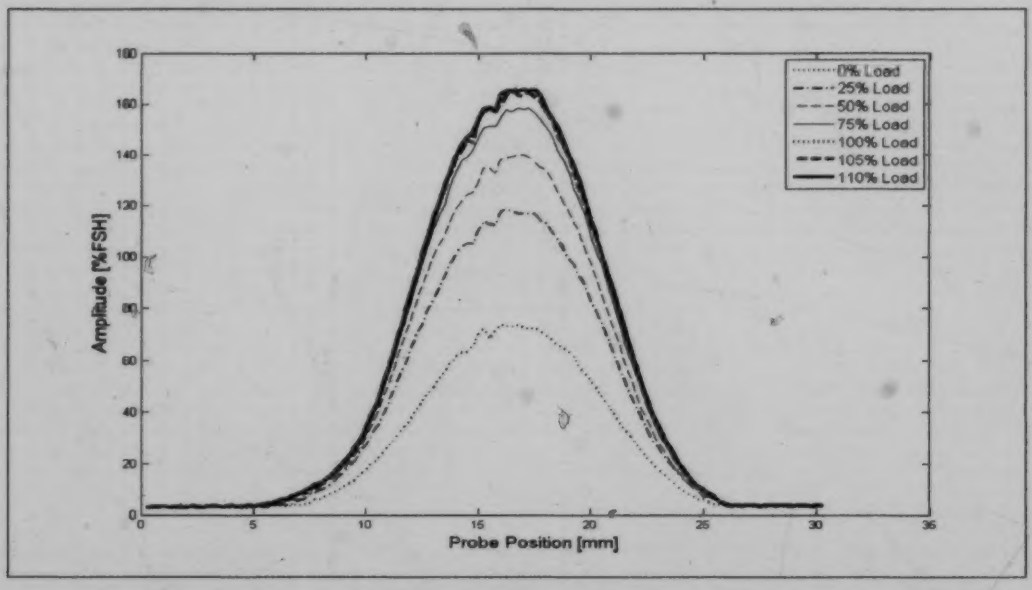

Figure 42: Extracted peak-to-peak amplitude from specimen CO2 at various crack opening loads

Similarly, specimen CO2 also displays the same trend for signal amplitude and loading level relationship. However, by observing the starting unloaded value of specimen CO2, it can be deduced that the unloaded and fully opened crack length of specimen CO2 is shorter than specimen CO1.

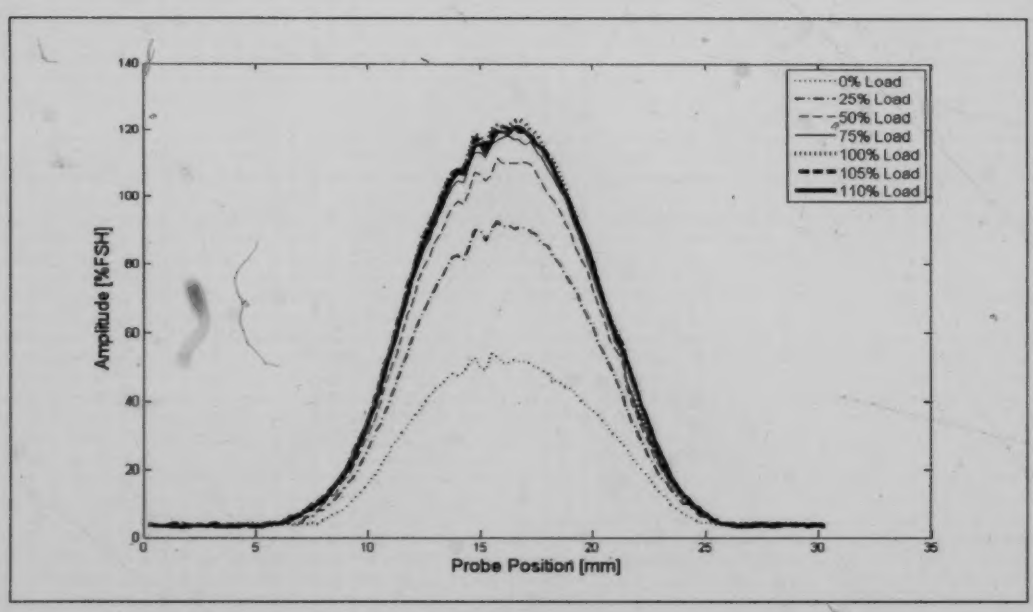

Figure 43: Extracted peak-to-peak amplitude from specimen CO3 at various crack opening loads

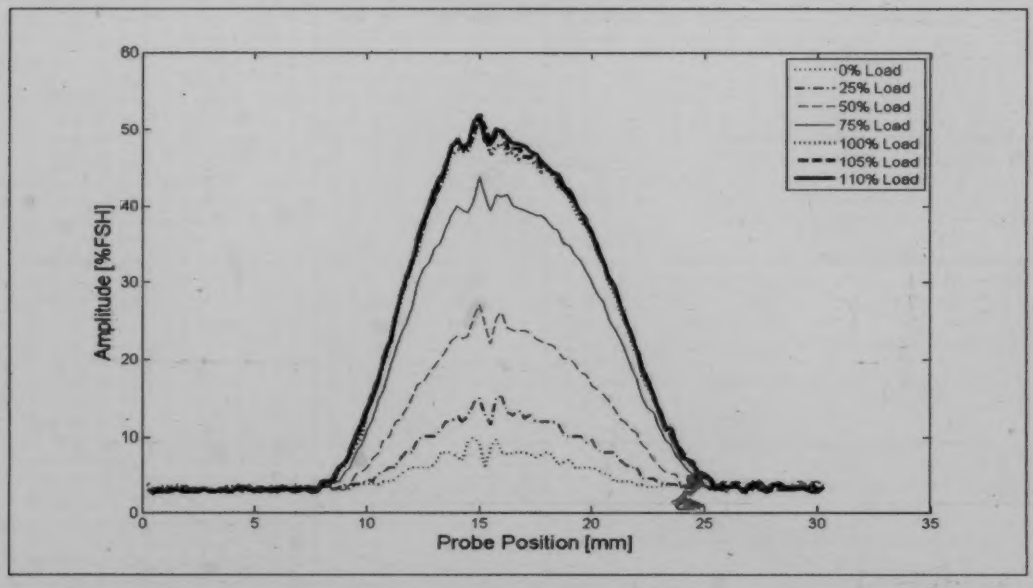

Figure 44: Extracted peak-to-peak amplitude from specimen CO4 at various crack opening loads

With similar observations on specimen CO3 and CO4, it can be deduced that on the basis of amplitude alone, a consistent relationship between crack opening load and ultrasonic signal amplitude can be established. Similar to the EDM specimens, the peak values of each specimen at all specified loading conditions are plotted to find the quantitative relationship between opening load and ultrasonic signal amplitude.

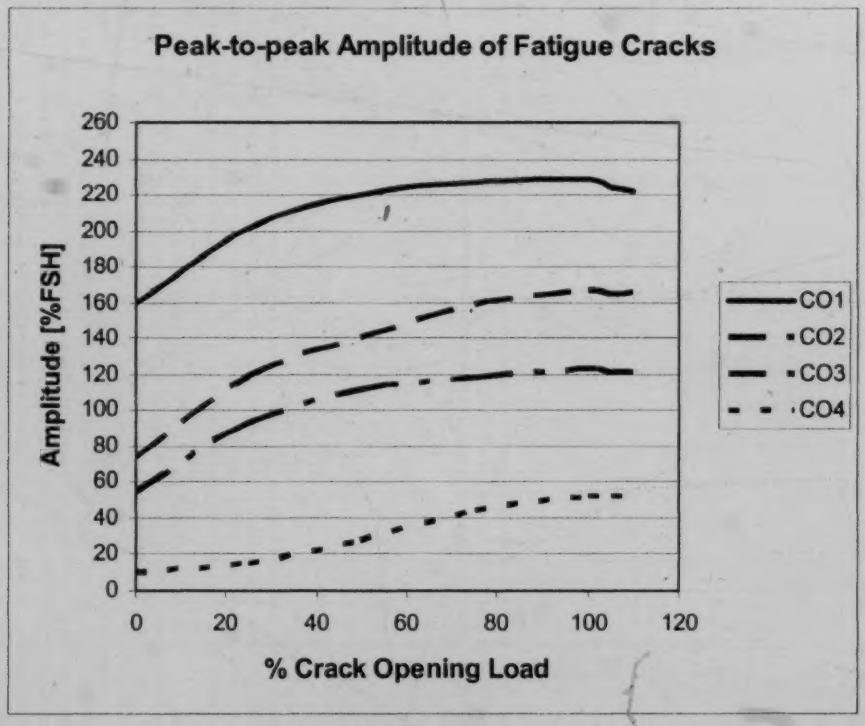

Figure 45: Peak-to-peak amplitude of fatigue cracks at various opening load levels

If the change in peak-to-peak amplitude of the ultrasonic signal obtained from EDM specimens, as shown in Figure 31, is assumed to be linear, the equation

that correlates the depth of a vertically oriented crack to the collected ultrasonic signal amplitude will be:

$$A_{peak-to-peak} = 39.896 \times a + 2.4671 \quad (8)$$

where:

$A_{peak-to-peak}$: Peak-to-peak amplitude

a : crack depth

Or, rearranging the formula to obtain crack depth from known amplitude yields:

$$a = \frac{\left(A_{peak-to-peak} - 2.4671\right)}{39.896} \quad (9)$$

Applying equation (9) to the fatigue crack peak-to-peak ultrasonic signal amplitude, the crack depths of each specimen at every crack opening load value can be estimated. Note that, although the actual crack depth of a specimen remains the same, the amount of crack closure or the applied opening load will change the effective crack depth that is 'visible' by the ultrasonic wave. The estimated average fatigue crack depths from 3 datasets for each specimen at different loading level are tabulated in Table 6.

Specimen (Measured Fatigue Crack Depth [mm])	Loading Level [% Full Crack Opening Load]	$A_{peak-to-peak}$ [%FSH]	Estimated Fatigue Crack Depth, a [mm]
CO1 (3.8735)	0	160.6	3.96
	25	201.8	4.99
	50	220.57	5.47

	75	227.23	5.63
	100	229.23	5.68
CO2 (3.048)	0	74.29	1.80
	25	118.83	2.92
	50	140.53	3.46
	75	159.27	3.93
	100	167.37	4.13
CO3 (2.0955)	0	54.21	1.29
	25	92.69	2.26
	50	111.4	2.73
	75	118.5	2.91
	100	123.17	3.03
CO4 (1.016)	0	10.37	0.2
	25	15.39	0.32
	50	27.11	0.62
	75	43.84	1.04
	100	51.53	1.23

Table 6: Fatigue crack depth estimation based on linear fitting of EDM specimens peak-to-peak amplitude of the ultrasonic signal reflected by the EDM slot corner

4.3.2 Data analysis on crack tip signal under various crack opening loads

The A-scan analysis of tip diffracted signal relies heavily on the B-scan. Using the B-scan, one can estimate the location of the tip signal without being confused by the surrounding noise due to the high gain level. Moreover, on the signal collection at 57.5 dB, B-scans show a constantly occurring signal that stays at the same position or time regardless of the probe position. This signal is known as the standing noise. It occurs due to the reflection from inside the wedge that manages to return to the probe's crystal. This signal is not clearly visible at gain level lower than approximately 32 dB. Similarly, the ultrasonic signal diffracted by the tip of the crack that can not be identified clearly at 25 dB gain is clearly noticeable at 57.5 dB gain. Crack tip signal can be observed by comparing the B-scan results obtained at different crack opening load levels. As opening load increases, the ultrasonic signal corresponding to the crack tip will move further away from the position of the crack corner signal. The progressions of crack tip signals obtained from specimen CO1 are shown in Figure 46 to Figure 52. Similar to the B-scans of EDM specimens, white solid ellipse indicates the crack tip diffracted signals, white dash ellipse represents the reflected signal from the corner of the crack and white rectangle is used to mark the standing noise due to the wedge of the angle beam transducer.

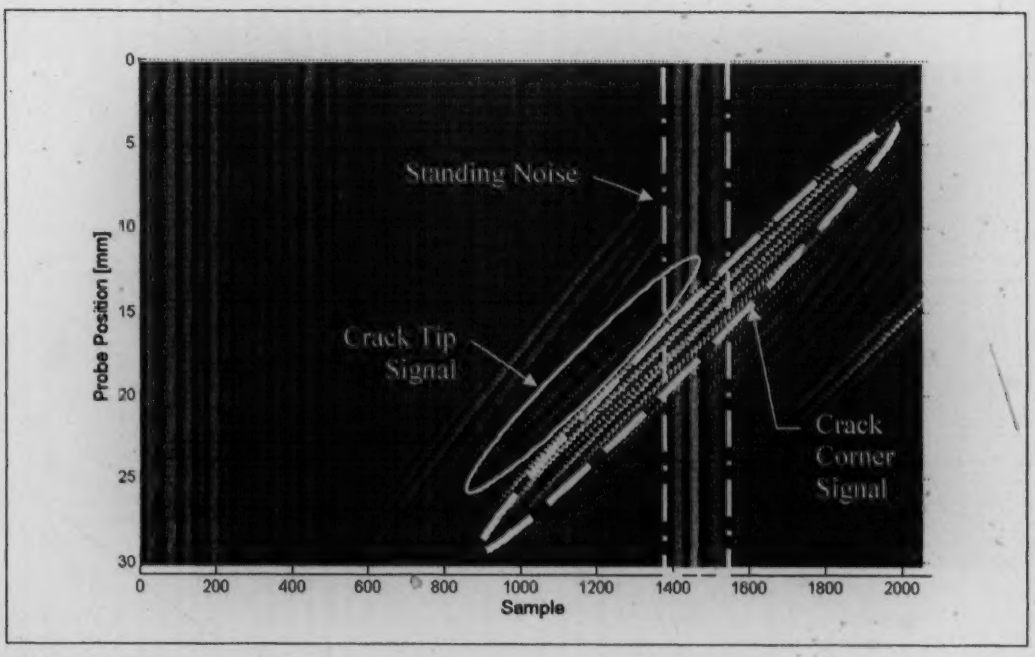

Figure 46: B-scans of specimen CO1 at no load

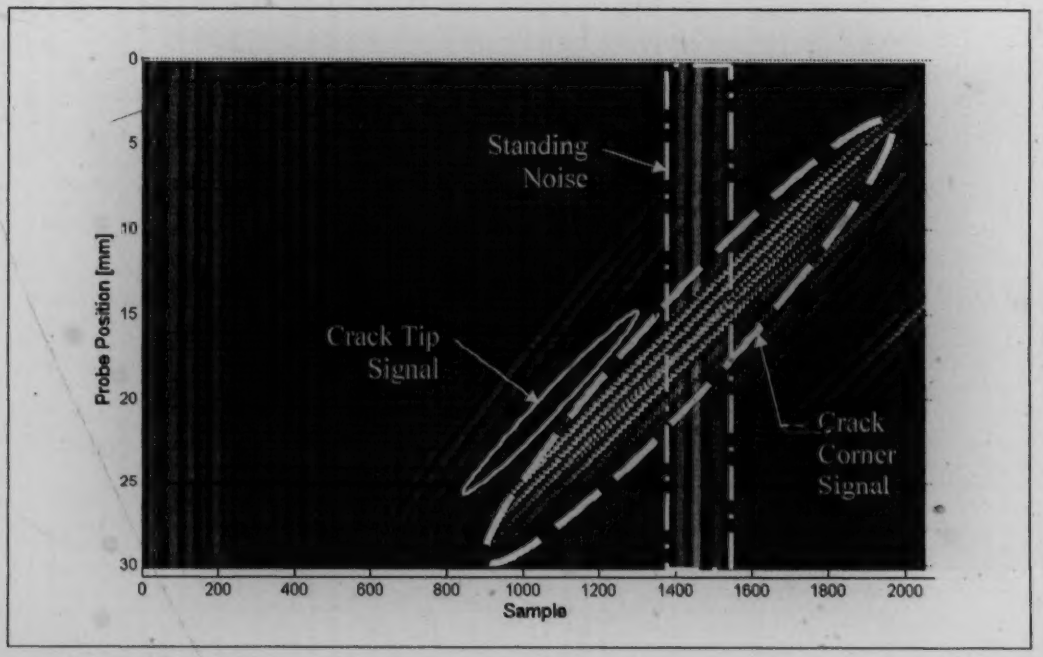

Figure 47: B-scans of specimen CO1 at 25% crack opening load

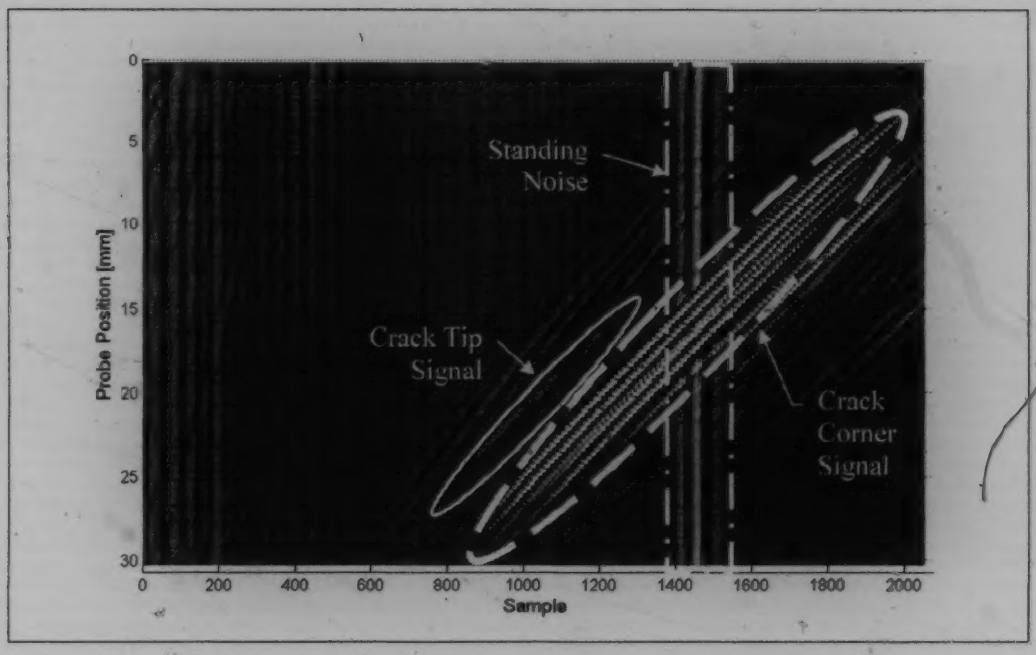

Figure 48: B-scans of specimen CO1 at 50% crack opening load

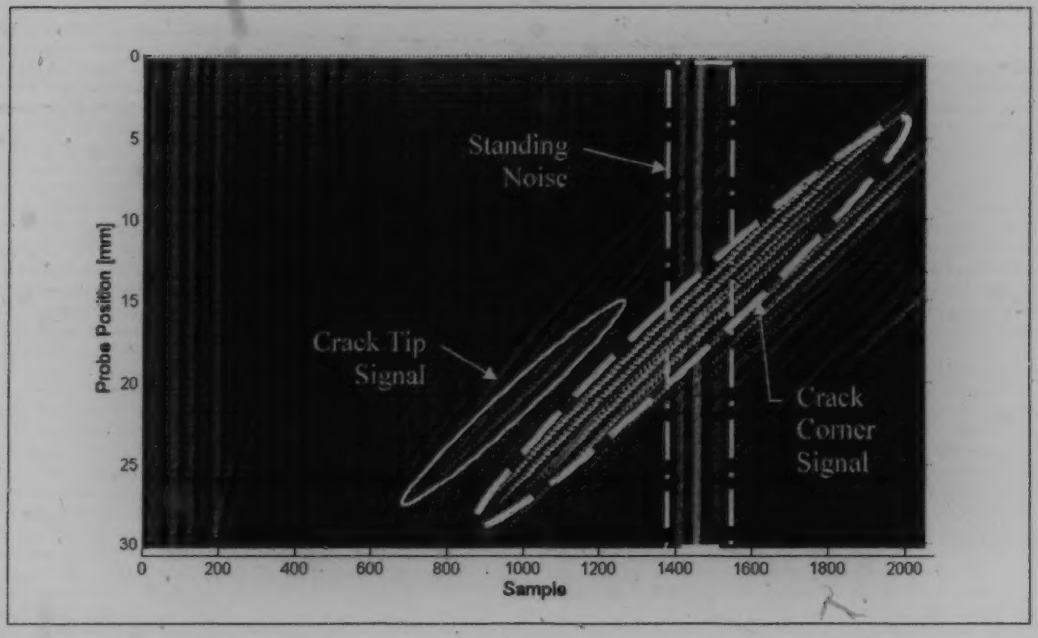

Figure 49: B-scans of specimen CO1 at 75% crack opening load

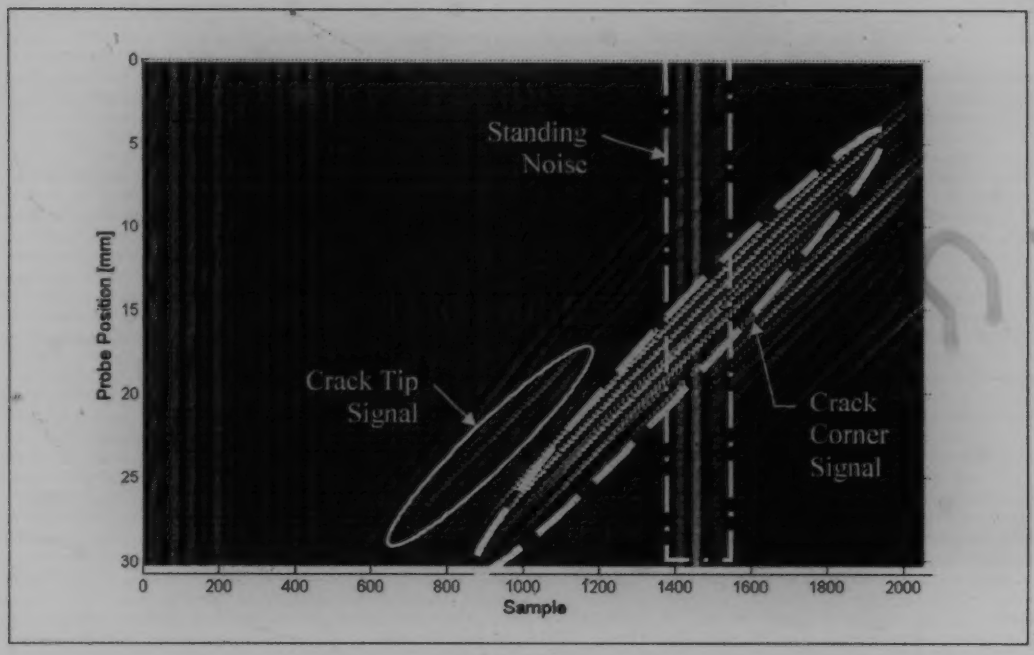

Figure 50: B-scans of specimen CO1 at 100% crack opening load

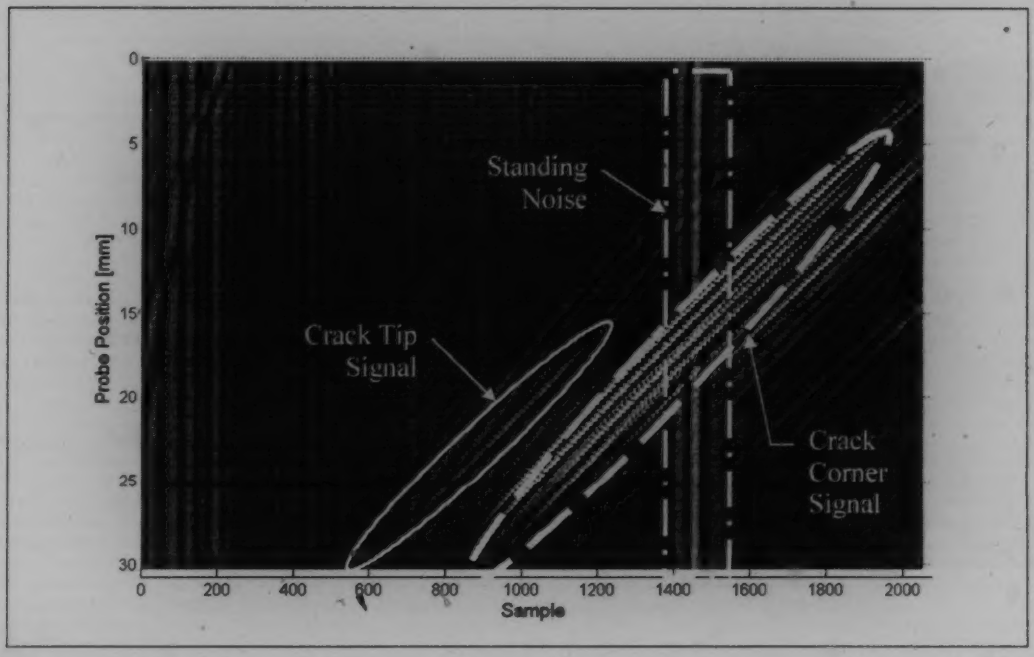

Figure 51: B-scans of specimen CO1 at 105% crack opening load

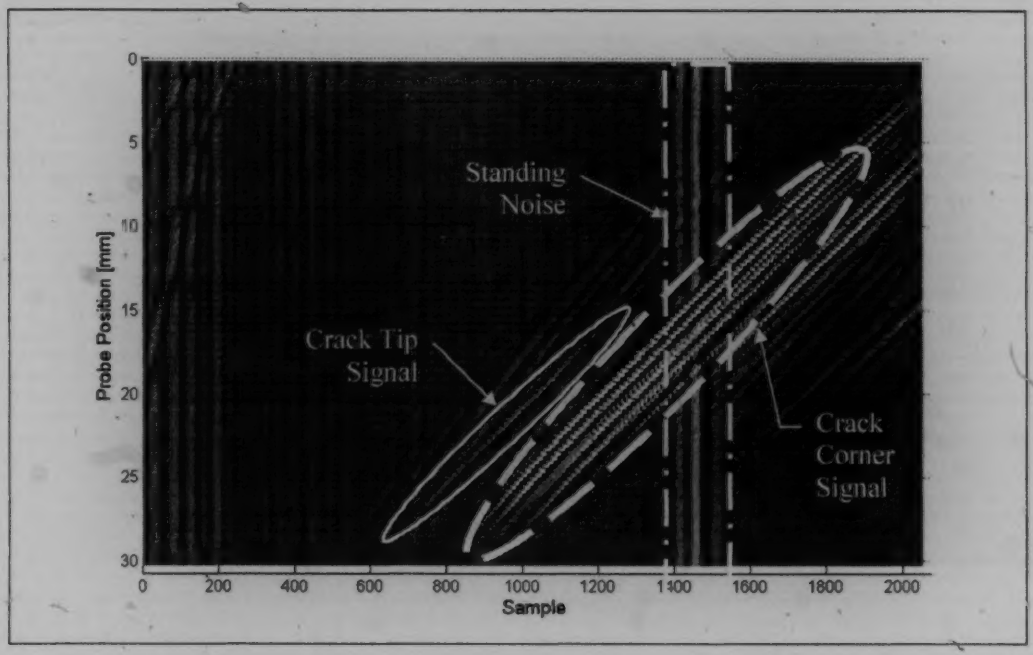

Figure 52: B-scans of specimen CO1 at 110% crack opening load

In order to estimate the sample number of the crack tip diffracted signal in A-Scan at a certain probe position, a grid is sketched on top of every B-scan in which the white solid ellipse marks the appearance of ultrasonic signal diffracted by the crack tip, the white horizontal lines identify the probe position and the white vertical lines represent the sample number. For example, in Figure 53, the corresponding sample number of positive peak of the crack tip diffracted signal at probe position of 25 mm is approximately 800. Therefore, when the A-Scan at probe position 25 mm is plotted as shown in Figure 54, it is easier to locate the crack tip diffracted signal from the noise and identify the probe position at which the crack tip diffracted signal begins to overlap with the ultrasonic signal reflected by the crack corner.

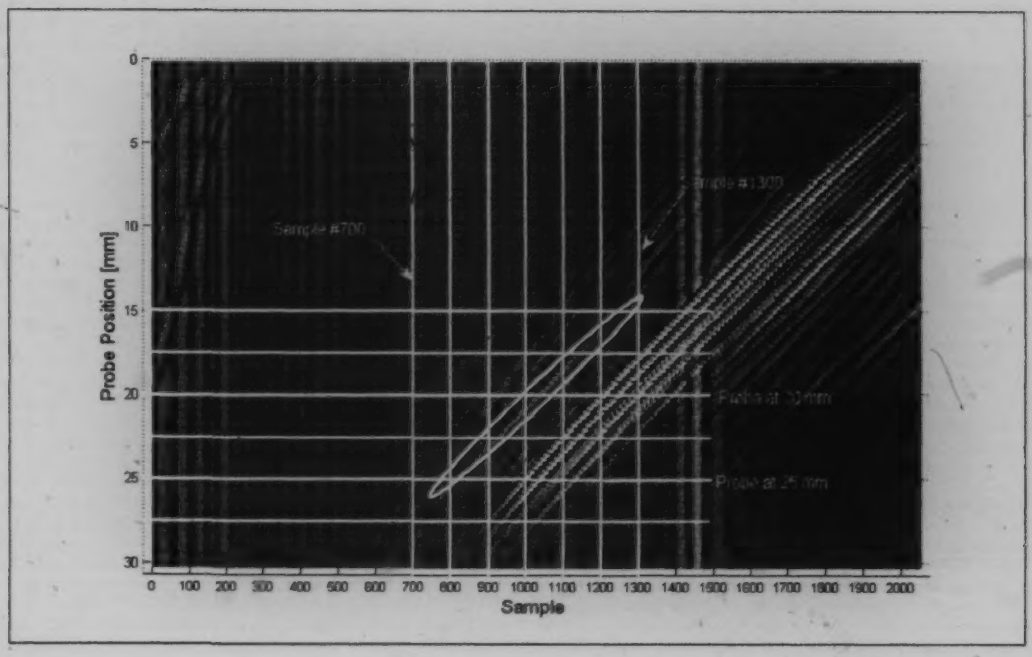

Figure 53: B-scans of specimen CO1 under 110% crack opening load

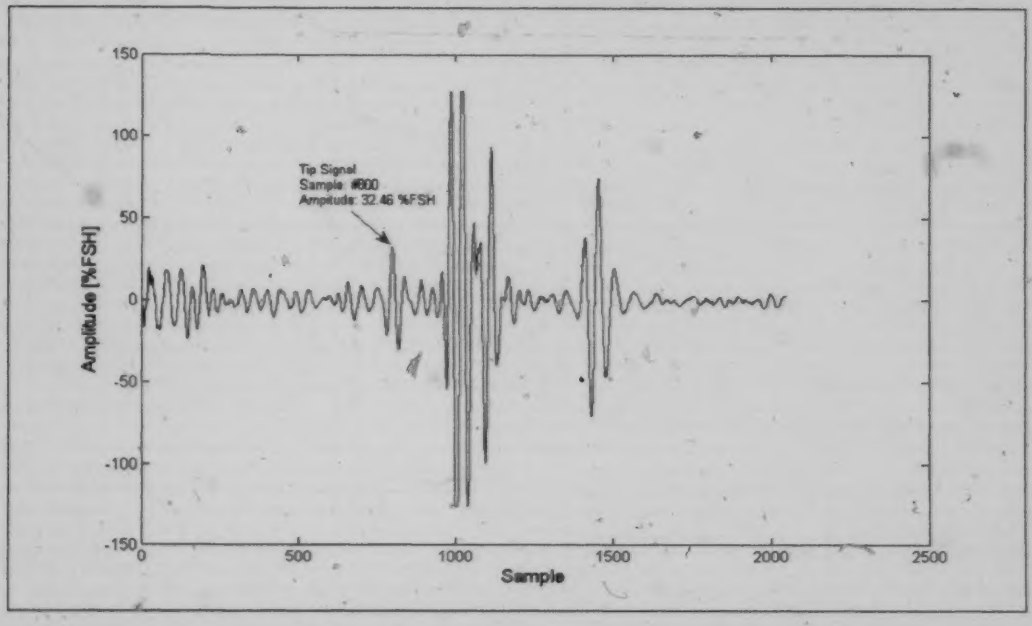

Figure 54: A-Scan of specimen CO1 under 110% crack opening load at probe position 25 mm.

By following the movement of the crack tip diffracted signal in the A-Scan from different probe positions, the time-of-flight, i.e., sample number, and amplitude of the tip signal are recorded and the subsequent echo-dynamics are presented in Figure 55 to Figure 57.

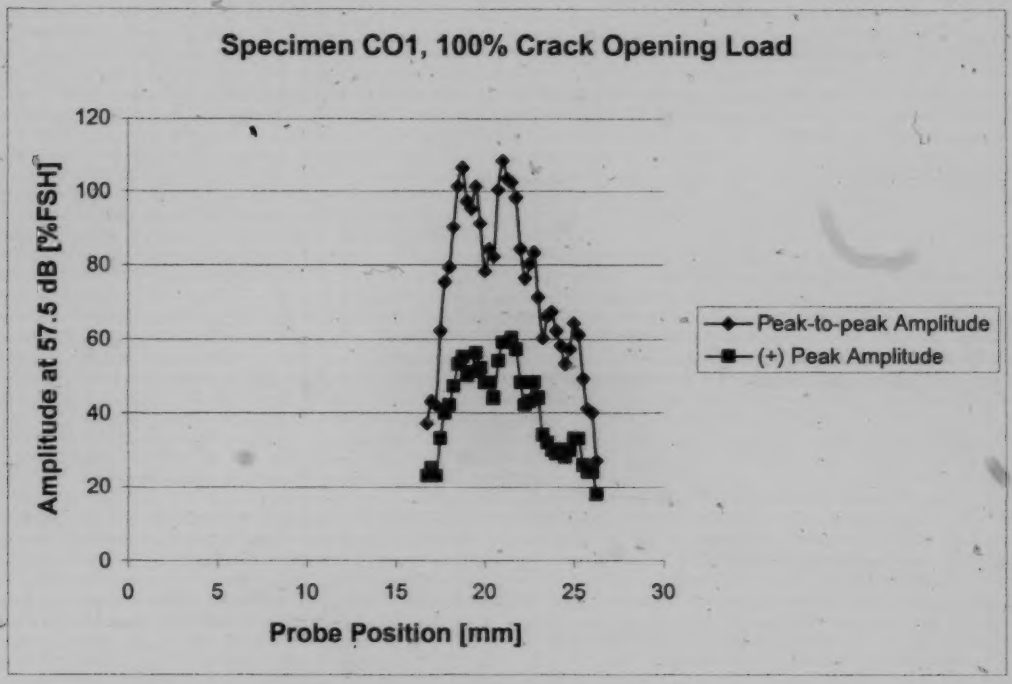

Figure 55: Extracted tip diffracted signal amplitude of specimen CO1 under 110% opening load

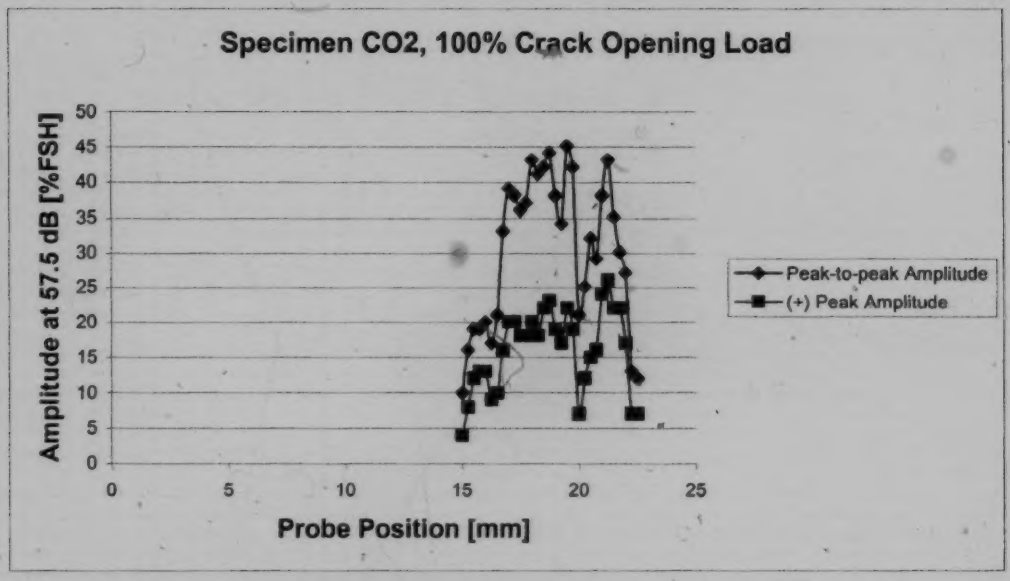

Figure 56: Extracted tip diffracted signal amplitude of specimen CO2 under 110% opening load

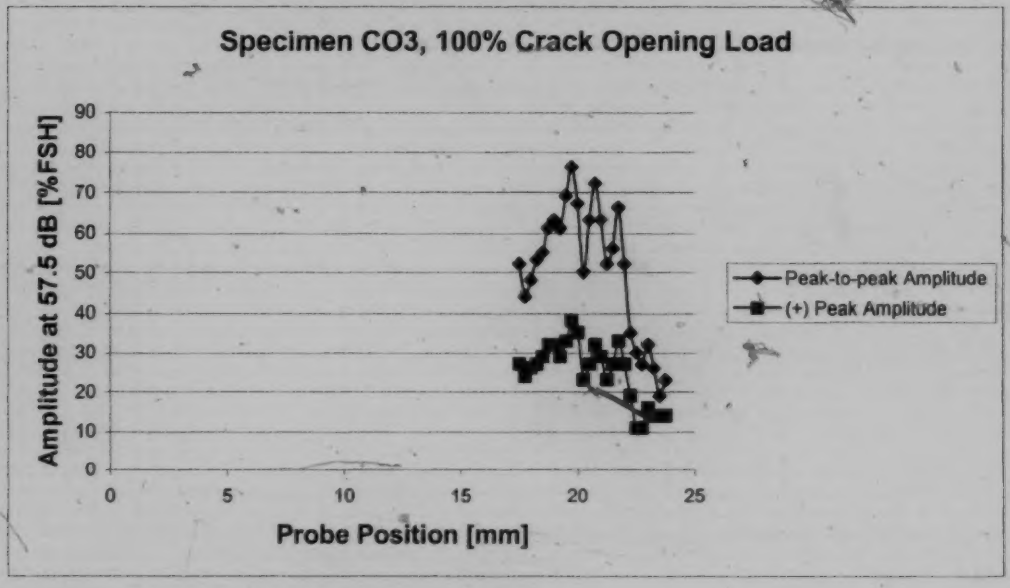

Figure 57: Extracted tip diffracted signal amplitude of specimen CO3 under 110% opening load

Note that, the echo-dynamics of specimen CO1 can not be obtained because most of the tip diffracted signal found in its B-Scan overlaps with the crack corner signal and thus, can not be distinguished reliably. Comparing the echo-dynamics of EDM specimens to fatigue crack specimens, it can be seen that the echo-dynamics of the latter show more than one peak amplitude. It is presumed that the multiple peaks on the echo-dynamics of the fatigue crack specimens occur due to the roughness of the surface of the fatigue crack, as opposed to the smoother surface of the EDM slot. As a result, this will make the estimation of the fatigue crack depths on the basis of the time-of-flight of the maximum amplitude of the crack tip diffracted signal more difficult, especially when the amplitudes of these multiple peaks are almost equivalent, as shown in Figure 55. The estimated fully open crack depths, i.e., under 100 % crack opening loads, using the calibrated x-axis of the Omniscan UT based on the detected peaks on the echo-dynamics is shown in Table 7. The crack depth formulation is identical to the one used for EDM slot depth estimation, i.e., $a = w - \left(n \times \frac{23.46\ mm}{2048} \right)$.

Specimen (Measured Fatigue Crack Depth [mm])	Probe Position [mm]	Maximum Amplitude [%FSH]	Sample Number	Estimated Fatigue Crack Depth [mm]	Average Estimated Fatigue Crack Depth [mm]
CO1 (3.8735)	18.75	113.45	1078	3.65	4.22
	21	113.44	978	4.79	

CO2 (3.048)	18	43.17	1187	2.40	3.0925
	18.75	44.17	1155	2.77	
	19.5	45.18	1122	3.15	
	21.25	43.17	1043	4.05	
CO3 (2.0955)	19.75	76.3	1120	3.17	3.42
	20.75	72.29	1076	3.67	

Table 7: Estimated fatigue crack depths under 100% crack opening load based on the calibrated axis of the Omniscan UT

Based on the crack depths' estimation in Table 7, there seems to be no definite values of crack depths that can be selected and thus, the calculated depths of each specimen from different probe positions are averaged. Note that, in the depth estimation of EDM slot, the graphical solution produces a more consistent answer with small error. Therefore, the same formula is used to estimate the fatigue crack depth under 100% crack opening load. The same peaks used in Table 7 are selected and the calculated fatigue crack depths are shown in Table 8.

Specimen (Measured Fatigue Crack Depth [mm])	Probe Position	Identified Sample Number	Estimated Fatigue Crack Depth [mm]	Estimated Average Fatigue Crack Depth [mm]
CO1 (3.8735)	18.75	1078	4.89	4.83
	21	978	4.77	
CO2	18	1187	3.47	3.435

(3.048)	18.75	1155	3.41	
	19.5	1122	3.39	
	21.25	1043	3.47	
CO3	19.75	1120	2.73	2.74
(2.0955)	20.75	1076	2.75	

Table 8: Estimated fatigue crack depths under 100% crack opening load using graphical solution

In the case of vertical defect growing from a specimen surface, there should be only one signal that corresponds to the tip of the defect, as previously shown in Figure 35 to Figure 38. But, the roughness of the crack surface leads to more amplitude variation and this leads to increasing difficulty in selecting the position of the crack tip signal. From Table 8, it can be seen that although several peaks whose amplitude are close to the maximum value are used, the calculated crack depths based on the graphical method do not deviate as much as those estimated using the calibrated axis of the Omniscan UT. Therefore, the graphical solution is found to yield a more consistent estimation.

In order to observe the effect of crack opening load on the collected ultrasonic signal, it is necessary to assess the effective crack depth in each loading level. The term effective crack depth refers to the crack area that do not experience any crack surface contact and hence, is not transparent to the ultrasonic beam. However, in some cases, the ultrasonic signal diffracted from the crack tip can not be detected reliably on the B-Scans. For specimens CO1 to CO3, the crack tip diffracted signals can be reliably detected in the B-Scans when at least 75%

crack opening load applied. Figure 58 to Figure 60 display the echo-dynamics of those specimens loaded at crack opening load lower than 75% whose crack tip signal can be observed clearly in the B-Scans. Using the graphical solution, the calculated depths of the fatigue cracks are shown in Table 9.

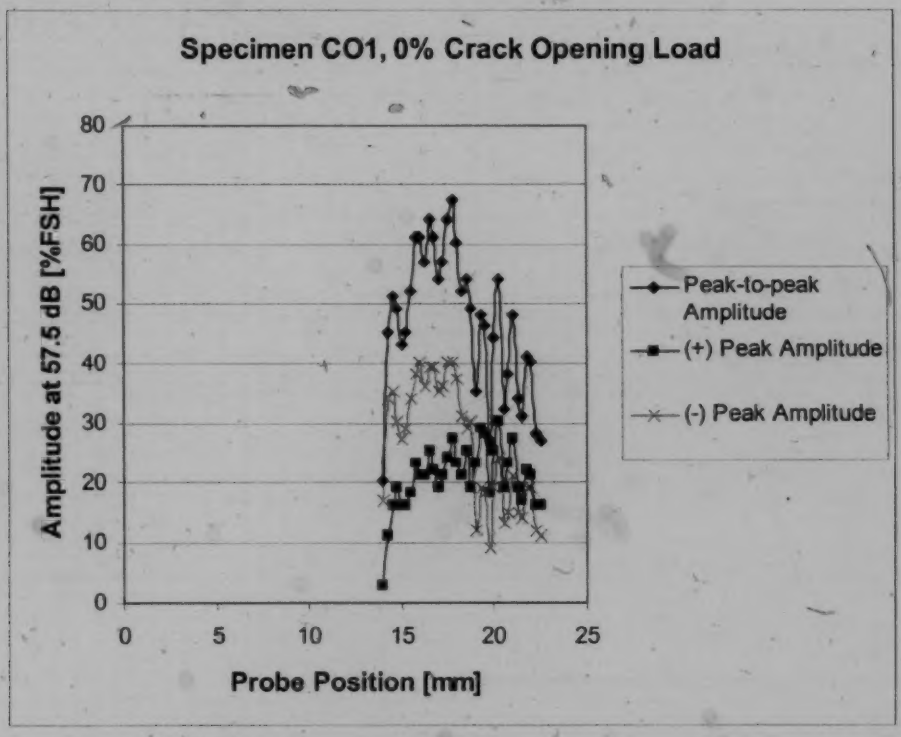

Figure 58: Echo-dynamics of ultrasonic signal diffracted by the crack tip of specimen CO1 under 0% crack opening load

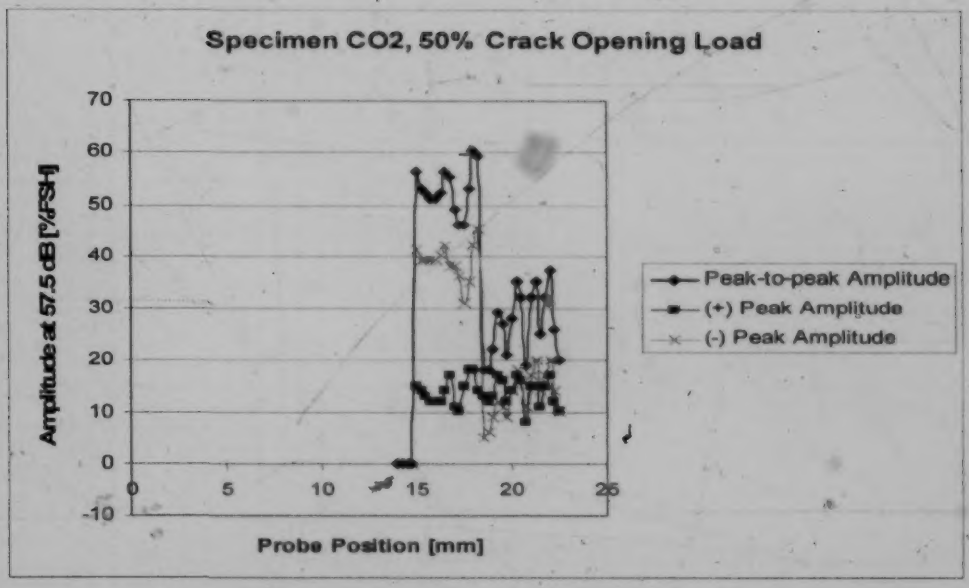

Figure 59: Echo-dynamics of ultrasonic signal diffracted by the crack tip of specimen CO2 under 50% crack opening load

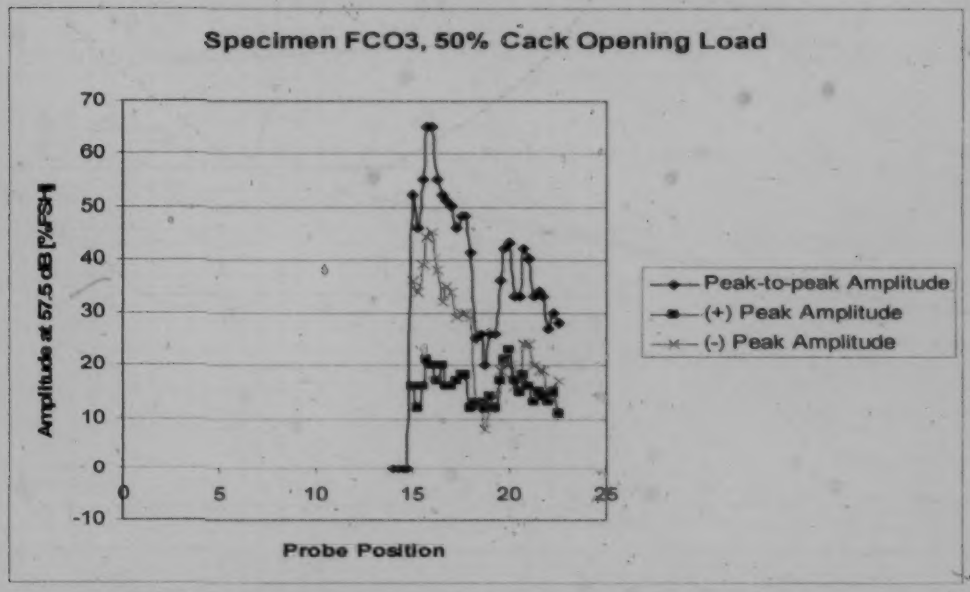

Figure 60: Echo-dynamics of ultrasonic signal diffracted by the crack tip of specimen CO3 under 50% crack opening load

Specimen (Measured Fatigue Crack Depth [mm])	% Load	Probe Position	Identified Sample Number	Estimated Fatigue Crack Depth [mm]	Average Estimated Fatigue Crack Depth [mm]
CO1 (3.8735)	0	16.5	1304	2.49	2.47
		17.75	1252	2.46	
		20.25	1114	2.46	
CO2 (3.048)	50	16.75	1276	2.76	2.72
		18	1222	2.64	
		20.25	1120	2.69	
		22	1044	2.79	
CO3 (2.0955)	50	16	1295	2.53	2.61
		20	1113	2.65	
		20.75	1083	2.65	

Table 9: Estimated crack depths under loading condition lower than 50% using graphical solution

Similar to the case of specimen under 100% loading, the estimated crack depths at different probe positions do not deviate very much from its average value and therefore, the results are more consistent. Moreover, the effect of crack surface contact on the ultrasonic signal is noticeable by comparing the calculated crack depths between Table 8 and Table 9. In the case of CO1 where the crack tip signal at 0% crack opening load can be analyzed, the difference in crack depth between unopened and fully opened condition is 51 %. This indicates that if such a crack in its natural state is being inspected without considering the effect of

crack surface contact, the measurement error may reach a value of 51% and it will be greatly undersized. Also, it can be seen that ultrasonic signal whether collected from the reflection due to the crack corner or from the diffraction due to the tip of the crack is sensitive in detecting the crack surface contact.

Chapter 5 Conclusion and Future Work

This thesis investigates the effect of crack surface contact on two key parameters of ultrasonic signal that are amplitude and time-of-flight. Ultrasonic nondestructive evaluations are conducted on the mild-steel plate specimen under no load condition and different levels of crack opening load. In order to analyze the collected data from fatigue crack specimens whose actual crack depths are unknown, it is necessary to obtain the ultrasonic data from specimens where the defects' depths and locations are known, i.e., EDM slots specimen. Using the amplitude data collected from different slot depths of EDM specimens, the actual crack depths of the fatigue crack specimens are estimated by comparing the extracted ultrasonic signal amplitude to the EDM specimens. Two distinct ultrasonic signals from different reflectors are used. The first one originates from the corner of the crack which is usually defined as crack mouth opening displacement. Signal collected from this area of the crack occurs due to reflection of the incoming ultrasonic waves and its direction greatly depends on the orientation of the crack. On the other hand, the ultrasonic signal that originates from the crack tip area takes place due to diffraction phenomena and thus, it is omni-directional.

Using the data collected from both reflectors, the effective depths of the fatigue cracks at no load condition and different loading levels up to fully open condition are estimated. The crack corner data shows high sensitivity toward different levels of externally applied crack opening load and shows that the crack surface

contact greatly affects the measurement results of ultrasonic NDE. Comparing the amplitude of the reflected signal between no load and fully open condition, it can be deduced that the effective crack depth decreases to as low as 50% of the actual crack depth when no load is applied.

In order to analyze the ultrasonic signal collected from the crack tip, it is necessary to distinguish the crack tip signal from the surrounding noise and thus, the use of B-Scan is a must. When 100% of crack opening loads are applied to the specimens, all the crack tip signals can be identified except for specimen CO4. This occurs due to the crack corner signal overlapping the crack tip signal. Between 0% and 100% opening load, the crack tip signal can also be identified from the B-scan results of specimen CO1, CO2 and CO3 at each crack opening level. However, due to the low signal to noise ratio, the crack tip features can not always be extracted from the A-scans when the specimens are subjected to 25% and 75% opening load.

Comparing the crack under no load and at fully opened condition, the effective crack depth at its natural state is found to be 51% of the actual crack depth and this confirms the conclusion from the amplitude based assessment. A graphical solution for crack depth estimation utilizes the time-of-flight of the crack tip and crack corner signal and is found to produce more consistent results compared to the depths estimation based on crack tip signal alone.

Note that all the fatigue cracks are generated under identical loading parameter and therefore, this leaves an area for possible research in the future. Also, all the data collected in this study is taken only from the centerline of the steel plate

specimen. Whether or not the ratio of the effective crack depth to the actual crack depth remain constant along the specimen width remains to be seen.

References

1. Ahmed, S.R. & Saka, M., "A Sensitive Ultrasonic Approach to NDE of Tightly Closed Small Cracks", Journal of Pressure Vessel Technology, 1998, Vol. 120, No. 4, pp. 384 – 392.
2. Ahmed, S.R. & Saka, M., "A New Ultrasonic Angle-beam Technique for Sensitive Evaluation of Closed Cracks", NDT & E International, 2000, Vol. 33, No. 4, pp. 261 – 271.
3. Ahmed, S.R. and Saka, M., "Quantitative Nondestructive Testing of Small Tight Cracks Using Ultrasonic Angle Beam Technique", Materials Evaluation, 2000, Vol. 58, No. 4, pp.564 – 574.
4. Ahmed, S.R. and Saka, M., "Ultrasonic Angle-Beam Technique as a Tool for Quantitative Characterization of Small Closed Cracks", The Japan Society of Mechanical Engineering International Journal, 2000, Series A, Vol. 43, No. 4, pp. 358 – 366.
5. Ahmed, S.R. and Saka, M., "Crack Length Independent Evaluation of Depth of Small Surface Cracks", Materials Evaluation, 2002, Vol. 60, No. 4, pp. 535 – 544.
6. Ahmed, S.R. and Saka, M., "Influence of Wall Thickness on the Ultrasonic Evaluation of Small Closed Surface Cracks and Quantitative NDE", Journal of Nondestructive Evaluation, 2002, Vol. 21, No. 1, pp. 9 – 22.
7. Akanda, M.A.S. and Saka, M., "Ultrasonic Shear Wave Technique for Sensitive Detection and Sizing of Small Closed Cracks", The Japan

Society of Mechanical Engineering Journal, 2002, Series A, Vol. 45, No. 2, pp. 252 – 261.

8. Akanda, M.A.S. and Saka, M., "Sensitive Ultrasonic Testing of a Small Closed Crack", Strength, Fracture and Complexity, 2003, Vol. 1, No. 2, pp. 89 – 99.
9. Akanda, M.A.S. and Saka, M., "Relationship between Closure Stress of Small Fatigue Crack and Ultrasonic Response", Journal of Nondestructive Evaluation, 2004, Vol. 23, No. 2, pp. 37 – 47.
10. Al-Nuamiy, W. and Zahran, O., "Time-of-flight Diffraction – From Semi-automatic Inspection to Semi-automatic Interpretation", Insight: Non-Destructive Testing and Condition Monitoring, 2005, Vol. 47, No. 10, pp. 639 – 644.
11. Anderson, T.L., Fracture Mechanics: Fundamentals and Applications, 3rd edition, Taylor & Francis Group, Boca Raton, USA, 2005.
12. Buck, O., Thompson, R.B., and Rehbein, D.K., "The Interaction of Ultrasound with Contacting Asperities: Applications to Crack Closure and Fatigue Crack Growth", Journal of Nondestructive Evaluation, 1984, Vol. 4, Nos. 3/4, pp. 203 – 208.
13. Budiansky, B. and Hutchinson, J.W., "Analysis of Closure in Fatigue Crack Growth", Journal of Applied Mechanics, 1978, Vol. 45, pp. 267 – 276.
14. Carman, C.D., Turner, C.C. and Hillberry, B.M., "A Method for Determining Crack Opening Load from Load – Displacement Data", Mechanics of Fatigue Crack Closure, ASTM STP 982, J.C. Newman, Jr. and W. Elber,

Eds., American Society for Testing and Materials, Philadelphia, 1988, pp. 214 – 221.

15. Chen, Que, Zhang and Liu, "Ultrasonic Nondestructive Testing Accurate Sizing and Locating Technique Based on Time-of-Flight –Diffraction Method", Russian Journal of Nondestructive Testing, 2005, Vol. 41, No. 9, pp. 594 – 601.

16. Ciorau, Scott, Gibbons and Blackney, "A Contribution to Detection and Sizing of Fatigue Cracks in Pipe Welds, Part 1: Time-of-flight diffraction techniques", Canadian Society of Nondestructive Testing, 1997, Vol. 18, No. 1, pp. 16 – 22.

17. Davidson, D.L., "Plasticity Induced Fatigue Crack Closure", Mechanics of Fatigue Crack Closure, ASTM STP 982, J.C. Newman, Jr. and W. Elber, Eds., American Society for Testing and Materials, Philadelphia, 1988, pp. 44 – 61.

18. Donald, J.K., "A Procedure for Standardizing Crack Closure Levels", Mechanics of Fatigue Crack Closure, ASTM STP 982, J.C. Newman, Jr. and W. Elber, Eds., American Society for Testing and Materials, Philadelphia, 1988, pp. 222 – 229.

19. Donald, J.K. and Phillips, E.P., "Analysis of the Second ASTM Round-Robin Program on Opening-Load Measurement Using the Adjusted Compliance Ratio Technique", Advances in Fatigue Crack Closure Measurement and Analysis: Second Volume, ASTM STP 1343, R.C.

McClung and J.C. Newman, Eds., American Society for Testing and Materials, Philadelphia, 1999, pp. 79 – 93.

20. Dwyer-Joyce, R.S., Drinkwater, B.W. and Quinn, A.M., "The Use of Ultrasound in the Investigation of Rough Surface Interfaces", Journal of Tribology, 2001, Vol. 123, No. 1, pp. 8 – 16.
21. Elber, W., "The Significance of Fatigue Crack Closure", Damage Tolerance in Aircraft Structures, ASTM STP 486, American Society for Testing and Materials, Philadelphia, 1971, pp. 230 – 247.
22. Fleck, N.A., "Compliance Methods for Measurement of Crack Length", Fatigue Crack Measurement: Techniques and Applications, K.J. Marsh, R.A. Smith and R.O. Ritchie, Engineering Materials, Advisory Services Ltd., West Midlands, UK, 1991, pp. 69 – 93.
23. Golan, S., Adler, L., Cook, K.V., Nanstad, R.K. and Bolland, T.K., "Ultrasonic Diffraction Technique for Characterization of Fatigue Cracks", Journal of Nondestructive Evaluation, 1980, Vol. 1, No. 1, pp. 11 – 18.
24. James, M.N. and Knott, J.F., "An Assessment of Crack Closure and the Extent of the Short Crack Regime in Q1N (HY80) Steel", Fatigue of Engineering Materials and Structures, 1985, Vol. 8, pp. 177 – 191.
25. Janssen, M., Zuidema, J., and Wanhil, R.J.H., Fracture Mechanics, 2nd edition, Spon Press, New York, USA, 2004.
26. Lidington, Silk, Montgomery and Hammond, "Ultrasonic Measurements of Depth of Fatigue Cracks", British Journal of Nondestructive Testing, 1976, Vol. 18, No. 6, pp. 165 – 170.

27. McEvily, A.J., "On Crack Closure in Fatigue Crack Growth", Mechanics of Fatigue Crack Closure, ASTM STP 982, J.C. Newman, Jr. and W. Elber, Eds., American Society for Testing and Materials, Philadelphia, 1988, pp. 35 – 43.

28. Mihara, T., Nomura, M., and Yamanaka, K., Relations between Crack Opening Behavior and Crack Tip Diffraction of Longitudinal Wave", Nondestructive Evaluation and Reliability of Micro- and Nanomaterial Systems, Proceedings of SPIE, 2002, Vol. 4703, pp. 137 – 145.

29. Mix, P.E., Introduction to Nondestructive Testing, John Wiley & Sons Inc., New York, USA, 1987.

30. Ramsay, D.C., Principles of Engineering Instrumentation, John Wiley & Sons Inc., New York, USA, 1996.

31. Rehbein, Van Wyk, Thompson and Buck, "Effect of Imperfect Interfaces on Acoustic Transmission and Diffraction", Review of Progress in Quantitative Nondestructive Evaluation, 1988, Vol. 7, pp. 1301 – 1310.

32. Saka, M. and Abe, H., "Sizing Closed Cracks by Ultrasonics and Analysis", Topics in Engineering, Computational and Experimental Fracture Mechanics, Developments in Japan, 1994, vol. 16, pp. 165 – 185.

33. Saka, M. and Akanda, M.A.S., "Ultrasonic Measurement of the Crack Depth and the Crack Stress Intensity Factor Under a No Load Condition", Journal of Nondestructive Evaluation, 2004, Vol. 23, No. 2, pp. 49 – 63.

34. Saka, Schneider and Holler "A New Approach to Detect and Size Closed Cracks by Ultrasonics", Research in Nondestructive Evaluation, 1989, Vol. 1, No. 2, pp. 65 – 75.

35. Saka, M. and Uchikawa, T., "Simplified NDE of a Closed Vertical Crack Using Ultrasonics", NDT & E International, 1995, Vol. 28, No. 5, pp.289 – 296.

36. Schijve, J., "Fatigue Crack Closure: Observations and Technical Significance", Mechanics of Fatigue Crack Closure, ASTM STP 982, J.C. Newman, Jr. and W. Elber, Eds., American Society for Testing and Materials, Philadelphia, 1988, pp. 5 – 34.

37. Shull, J.P., Nondestructive Evaluation: Theory, Techniques, and Applications, Marcel Dekker Inc., New York, USA, 2002.

38. Silk, M.G., "Sizing Crack-like Defects by Ultrasonic Means", Research Techniques in Nondestructive Testing, Vol. 3, ed, by R.S. Sharpe, Academic Press Inc., New York, USA, 1977.

39. Silk, M.G., "The Transfer of Ultrasonic Energy in the Diffraction Technique for Crack Sizing", Ultrasonics, 1979, Vol. 17, No. 3, pp. 113 – 121.

40. Silk, M.G., "Use of Diffraction-based Time-of-flight Measurements to Locate and Size Defects", British Journal of Nondestructive Testing, 1984, Vol. 26, No. 4, pp. 208 – 213.

41. Silk, M.G., "Change in Ultrasonic Defect Location and Sizing", NDT International, 1987, Vol. 20, No. 1, pp. 9 – 14.

42. Silk, M.G. and Lidington, B.H., "Defect Sizing using an Ultrasonic Time Delay Approach", British Journal of Non-destructive Testing, 1975, Vol. 17, No. 2, pp. 33 – 36.

43. Thomas, R., Drinkwater, B.W. and Liaptsis, D., "The Reflection of Ultrasound from Partially Contacting Rough Surfaces", The Journal of the Acoustical Society of America, 2005, Vol. 177, No. 2, pp. 638 – 645.

44. Wheeler, A.J. and Ganji, A.R., Introduction to Engineering Experimentation, 2nd edition, Pearson Education Inc., New Jersey, USA, 2004.